HHS Public Access

Author manuscript

Cell Rep. Author manuscript; available in PMC 2019 September 25.

Published in final edited form as:

Cell Rep. 2019 September 10; 28(11): 2824–2836.e8. doi:10.1016/j.celrep.2019.08.011.

Fascin Controls Metastatic Colonization and Mitochondrial Oxidative Phosphorylation by Remodeling Mitochondrial Actin Filaments

Shengchen Lin[1], **Chongbiao Huang**[2], **Venugopal Gunda**[3], **Jianwei Sun**[1,4], **Srikumar P. Chellappan**[5], **Zengxun Li**[2], **Victoria Izumi**[6], **Bin Fang**[6], **John Koomen**[6], **Pankaj K. Singh**[3], **Jihui Hao**[2], **Shengyu Yang**[1,5,7,*]

[1]Department of Cellular and Molecular Physiology, Penn State College of Medicine, Hershey, PA, USA

[2]Department of Pancreatic Cancer, Tianjin Medical University Cancer Institute and Hospital, National Clinical Research Center for Cancer, Key Laboratory of Cancer Prevention and Therapy, Tianjin 300060, China

[3]Eppley Institute for Research in Cancer and Allied Diseases, Department of Pathology and Microbiology, University of Nebraska Medical Center, Omaha, NE, USA

[4]State Key Laboratory of Conservation and Utilization of Bio-Resources in Yunnan and Center for Life-Sciences, School of Life Sciences, Yunnan University, Kunming, China

[5]Department of Tumor Biology, H. Lee Moffitt Cancer Center, Tampa, FL, USA

[6]Department of Molecular Oncology and Proteomics Core, H. Lee Moffitt Cancer Center, Tampa, FL, USA

[7]Lead Contact

SUMMARY

The deregulation of the actin cytoskeleton has been extensively studied in metastatic dissemination. However, the post-dissemination role of the actin cytoskeleton dysregulation is poorly understood. Here, we report that fascin, an actin-bundling protein, promotes lung cancer metastatic colonization by augmenting metabolic stress resistance and mitochondrial oxidative phosphorylation (OXPHOS). Fascin is directly recruited to mitochondria under metabolic stress to stabilize mitochondrial actin filaments (mtF-actin). Using unbiased metabolomics and proteomics

*Correspondence: sxy99@psu.edu.

AUTHOR CONTRIBUTIONS

S.Y. and S.L. conceived the present study and analyzed most of the data. S.Y. and S.L. wrote the manuscript with input and support from all authors. S.L. performed most of the experiments. C.H., Z.L., and J.H. performed IHC staining and analyzed the results. V.G. and P.K.S. performed the metabolomics screening and analyzed the results. V.I., B.F., and J.K. performed the proteomics and analyzed the results. J.S. performed the initial experiment linking fascin and mtF-actin to mtDNA. S.P.C. provided critical reagents and technical support.

SUPPLEMENTAL INFORMATION

Supplemental Information can be found online at https://doi.org/10.1016/j.celrep.2019.08.011.

DECLARATION OF INTERESTS

The authors declare no conflict of interest.

approaches, we discovered that fascin-mediated mtF-actin remodeling promotes mitochondrial OXPHOS by increasing the biogenesis of respiratory Complex I. Mechanistically, fascin and mtF-actin control the homeostasis of mtDNA to promote mitochondrial OXPHOS. The disruption of mtF-actin abrogates fascin-mediated lung cancer metastasis. Conversely, restoration of mitochondrial respiration by using yeast NDI1 in fascin-depleted cancer cells is able to rescue lung metastasis. Our findings indicate that the dysregulated actin cytoskeleton in metastatic lung cancer could be targeted to rewire mitochondrial metabolism and to prevent metastatic recurrence.

Graphical Abstract

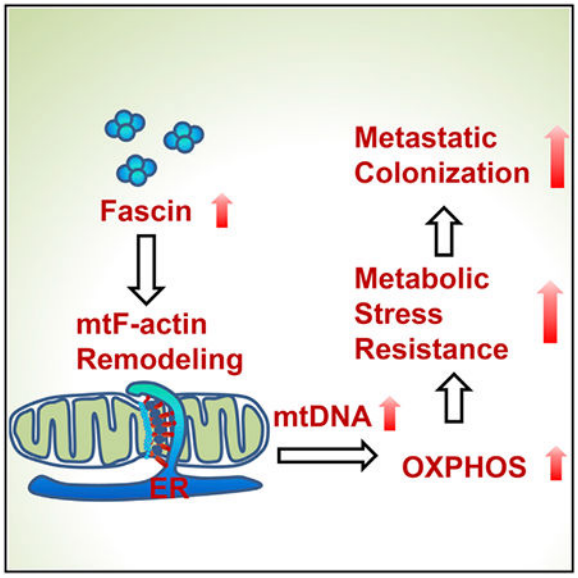

In Brief

Lin et. al. show that fascin, a prometastasis actin-bundling protein, promotes mitochondrial oxidative phosphorylation and metabolic stress resistance in lung adenocarcinoma by remodeling mitochondrial actin filaments and regulating the homeostasis of mitochondrial DNA.

INTRODUCTION

The organization of actin filaments into bundles and networks is essential for the diverse cellular functions of the actin cytoskeleton. Fascin is a pro-metastasis actin-bundling protein required for the maximal crosslinking of F-actin into straight and rigid bundles (Tilney et al., 1998). Fascin overexpression invariably correlates with aggressive clinical course, metastatic progression, and shorter survival across different types of carcinoma (Hashimoto et al., 2005; Pelosi et al., 2003). It is generally believed that fascin plays a mechanical role in driving tumor cell migration and invasion by facilitating membrane protrusions. However, there is also evidence implicating fascin in oncogenesis (Scott et al., 2011), metastatic colonization(Li et al., 2014), anoikis resistance, chemoresistance, and cancer cell stemness (Barnawi et al., 2016). Molecular mechanisms underlying these non-canonical functions of fascin are not clear.

Mitochondria are highly dynamic powerhouses of the cell constantly undergoing fission and fusion (Friedman and Nunnari, 2014). The division of mitochondria is initiated by constriction of the mitochondrial fission site by the endoplasmic reticulum (ER) tubule and followed by membrane scission mediated by the dynamin-related protein 1 (Drp1) (Friedman et al., 2011; Ji et al., 2015; Korobova et al., 2013; Manor et al., 2015). The ER-anchored inverted formin 2-CAAX (INF2-CAAX) facilitates the polymerization of F-actin at the ER-mitochondrion contacts, which provides mechanical forces for the initial mitochondrial constriction (Ji et al., 2015; Korobova et al., 2013). Cortactin, Arp2/3 complex, myosin II, and several other actin regulatory proteins are also implicated in the assembly and regulation of mitochondrial F-actin (De Vos et al., 2005; Li et al., 2015; Manor et al., 2015). It is unclear whether or how the actin cytoskeleton dysregulation during metastatic progression might affect mitochondrial actin filaments (mtF-actin) or mitochondrial metabolism.

Here, we report a role of fascin in the control of metastatic colonization and mitochondrial oxidative phosphorylation (OXPHOS) by remodeling mtF-actin. Our findings implicate that the dysregulation of the actin cytoskeleton in post-dissemination cells is able to control lung cancer metastasis by rewiring mitochondrial metabolism. Small molecule inhibitors targeting fascin could be potentially used to prevent metastatic recurrence by reprogramming mitochondrial metabolism.

RESULTS

Fascin Is Required for Metastatic Colonization and Metabolic Stress Resistance

Our immunohistochemistry analysis of lung cancer patient specimens supported that fascin expression was highly elevated in lung adenocarcinoma patients (Figures 1A and 1B). Fascin overexpression was associated with larger tumor size, lymph node involvement, advanced staging, and shorter survival (Figure 1C; Table S1). To understand the role of fascin in lung cancer metastasis, we used short hairpin RNA (shRNA) or CRISPR/Cas9 to deplete the expression of fascin in lung adenocarcinoma cells (Figure S1A). Depletion of fascin blocked the tumor metastasis of tail-vein-injected H292 cells, implicating a causal role of fascin in metastatic colonization (Figures 1D and 1E).

Next, we investigated whether fascin has a post-dissemination role in lung cancer metastasis. Because the extravasation of cancer cells from the microvasculature is dependent on cell mobility and invasiveness, we used inducible CRISPR/Cas9 to interrogate the post-extravasation function of fascin in metastatic expansion. In this system, doxycycline induced the expression of Cas9 and the depletion of fascin protein in about 7 days (Figure S1B). Luciferase-labeled Lewis lung cancer (LLC) cells stably expressing Tet-On Cas9 and fascin single-guide RNA (sgRNA) were injected into albino BL6 mice by tail vein. Forty-eight hours after tail-vein injection, the mice were fed with doxycycline chow to induce the expression of Cas9 and the deletion of fascin (Figure 1F). At 48-h post-tail-vein injection, more than 95% of LLC cells had already extravasated to the lung parenchyma (Figures S1C and S1D). Depletion of fascin in post-extravasation LLC cells dramatically inhibited the development of LLC lung metastases (Figures 1G and 1H; Figure S1E). Only micrometastases were detected in the lung after inducible depletion of fascin in post-

dissemination LLC cells (Figure S1F). In contrast, fascin knockout (KO) was only able to marginally inhibit the tumor growth of subcutaneous LLC xenograft (Figure S1G; n = 10, p = 0.08), suggesting that fascin is more critical for metastatic expansion than for primary tumor growth. Immunohistochemistry (IHC) analysis indicated that residual micro-metastases in the lung were positive for fascin expression, indicating these residual micro-lesions might be due to incomplete depletion of fascin (Figure S1H). Pharmacological inhibition of fascin using the small molecule inhibitor G2 (Huang et al., 2015 in post-extravasation LLC cells was also able to markedly inhibit metastatic expansion (Figures 1I and 1J). Taken together, our data suggest fascin is required for the metastatic expansion of disseminated lung cancer cells, which could be potentially targeted to prevent metastatic recurrence.

Overcoming metabolic stress is crucial for disseminated cancer cells to establish distant metastases. The glucose concentration in the tumor microenvironment is as much as 10 times lower than in the normal tissue (Birsoy et al., 2015; Liu et al., 2016. Glucose uptake is also dramatically inhibited when cancer cells lose adhesion to the extracellular matrix (e.g., circulating tumor cells), which results in oxidative stress and anoikis (Schafer et al., 2009). Therefore, we examine the effects of fascin KO and knockdown on non-small cell lung cancer (NSCLC) cell proliferation under regular cell culture conditions (10 mM glucose [Glc]) and glucose-limited conditions (1 mM glucose). Fascin depletion with CRISPR/Cas9 or shRNA had no effect on lung cancer cell proliferation under a physiological concentration of glucose (10 mM) (Figure 1K; Figures S1I and S1J). However, when the glucose availability was limited (1 mM glucose), the proliferation of fascin-depleted cells was significantly slower (Figures 1K, S1I, and S1J). Fascin depletion also remarkably inhibited soft agar colony formation and resistance to cell death induced by biguanide metabolic drug phenformin (Figures 1L–1N). Conversely, fascin overexpression in NSCLC cells remarkably promoted cell proliferation and survival under metabolic stresses (glucose limitation, loss-of-adhesion, and phenformin treatment) (Figures 1K, 1L, and 1N; Figures S1I–S1J), suggesting that fascin overexpression in NSCLC promotes metabolic stress resistance to facilitate metastatic colonization.

Fascin Overexpression Promotes Mitochondrial OXPHOS in Lung Cancer Cells

In order to understand the mechanism by which fascin controls metabolic stress resistance, we analyzed the levels of approximately 280 polar metabolites in control and fascin KO H1650 cells by using liquid chromatography-tandem mass spectrometry (LC-MS/MS). The metabolome of the fascin KO group clustered distinctly from that of control cells (Figure S2A). The most significantly altered metabolic pathways in fascin KO cells included nicotinamide metabolism, glutathione, and methionine metabolic pathways (Figure 2A; Figures S2B and S2C). The TCA (tricarboxylic acid) cycle was also among the altered metabolic pathways in fascin-depleted lung cancer cells (Figure 2A). We confirmed that fascin KO decreased NAD+ and NADH levels (Figure 2B), suggesting a critical role for fascin in NSCLC nicotinamide homeostasis.

Mitochondrial respiration is crucial for nicotinamide metabolism (Birsoy et al., 2015; Sullivan et al., 2015) and metabolic stress resistance (Birsoy et al., 2015; Liu et al., 2016;

Sullivan et al., 2015). To determine whether fascin might control mitochondrial metabolism, we performed stable isotope tracing analysis by incubating control or fascin KO H1650 cells with [U-^{13}C]-glucose. The incorporation of ^{13}C to a targeted panel of TCA cycle metabolites in the cell was then analyzed using LC-MS. As shown in Figures 2C and 2D, there was about a 30%–50% decrease in the levels of M+2 α-ketoglutarate aconitate, citrate and isocitrate, fumarate, malate, and glutamate; in contrast, the levels of M+2 acetyl-coenzyme A (CoA) increased by about 2-fold, suggesting inhibition of metabolic flux to the TCA cycle in fascin-depleted cells. To further determine the role of fascin in mitochondrial metabolism, we used a mito-stress test to evaluate the effects of fascin depletion or overexpression on mitochondrial oxygen consumption rate in lung cancer cells. As shown in Figures 2E and 2F; Figures S2D and S2E, fascin depletion with CRISPR/Cas9 or shRNA dramatically inhibited basal, ATP-linked, and maximal oxygen consumption rates (OCRs) in all the tested NSCLC cells. Conversely, fascin overexpression in NSCLC cells remarkably increased mitochondrial OCR, strongly supporting an essential role for fascin in mitochondrial OXPHOS (Figures 2G and 2E ; Figure S2F). To determine whether the ability to promote mitochondrial respiration is specific to fascin, we overexpressed fimbrin, another actin-bundling protein with similar actin crosslinking properties to fascin, in H1650 cells. The overexpression of fimbrin had no effects on mitochondrial OXPHOS (Figures S2G and S2H). Taken together, our data support that fascin overexpression in lung cancer is able to enhance mitochondrial OXPHOS.

Fascin Controls OXPHOS by Remodeling mtF-Actin

To understand the mechanism by which fascin controls OXPHOS, we first asked whether fascin regulates mitochondrial metabolism through its actin-bundling activity. According to the crystal structure and mutagenesis studies of fascin (Chen et al., 2010; Sedeh et al., 2010), there are two major actin-binding sites in the fascin structure (Lin et al., 2016; Yang et al., 2013). Two of the fascin mutants (S39E at site 1 and R149A/K150A/R151A, or 149-151A for short, at site 2) have lost bundling activity without changing the global protein structure (Yang et al., 2013). When expressed in fascin knockdown H1650 cells, wild-type fascin was able to rescue mitochondrial OCRs and NAD+ and NADH levels (Figures 3A–3D; Figure S3A). Mutations at the two separate actin-binding sites completely abrogated the ability of fascin to restore mitochondrial OCRs and nicotinamide levels (Figures 3A–3D), suggesting that fascin regulates mitochondrial metabolism through actin crosslinking.

The mtF-actin has recently been implicated in mitochondrial dynamics (De Vos et al., 2005; Ji et al., 2015; Korobova et al., 2013, 2014; Li et al., 2015; Manor et al., 2015), although the role of mtF-actin in cancer metabolism is unknown. Because fascin-mediated control of mitochondrial metabolism depends on its actin-bundling activity, we evaluated the effects of fascin depletion on mtF-actin accumulation in NSCLC cells. Mitochondria in NSCLC cells have very diverse morphologies, ranging from bead-like, fragmented structures (in LLC cells) and inter-connected networks spreading throughout the cell (H1650 cells) to thread-like structures mostly concentrated on one side of the nucleus (in H23 cells) (data not shown). When F-actin was stained with phalloidin, we observed constitutive mtF-actin accumulated at bead-like mitochondria in the majority of LLC cells (>80%) under regular cell culture conditions (Figures 2E and 2F). Fascin depletion in LLC cells resulted in

elongated mitochondria and reduced the proportion of mtF-actin-positive cells to approximately 20% (Figures 2E and 2F). No mtF-actin was observed in H23 under conventional cell culture conditions (Figure S3B). However, treatment of H23 cells with glucose limitation (1 mM glucose) or trifluoromethoxy carbonylcyanide phenylhydrazone (FCCP) induced mitochondrial fragmentation and accumulation of mtF-actin in 50%–100% of cells, which was abrogated by the depletion of fascin (Figure 3G; Figures S3B and S3C). We were not able to evaluate mtF-actin in H1650 and H292 cells due to strong background staining of F-actin in these cells (data not shown). Taken together, our data implicate a crucial role for fascin in metabolic-stress-induced mtF-actin accumulation.

To determine whether fascin might be directly recruited to regulate mtF-actin under metabolic stress, we examined the effects of metabolic stress on the localization of fascin in lung cancer cells. No localization of EGFP-fascin was observed in H23 cells cultured in medium containing 10 mM glucose (Figure S3D). However, glucose limitation (1mM glucose) induced robust recruitment of fascin to fragmented mitochondria in H23 cells (Figures 3H and 3I). Interestingly, shRNA depletion of INF2-CAAX (an ER-anchored splicing variant of INF2 that is responsible for ER-originated mtF-actin assembly) was able to abrogate the recruitment of fascin to mitochondria under glucose limitation (Figures 3H and 3I; Figure S3E). Mitochondrial stress induced by FCCP was also able to induce strong mitochondrial recruitment of fascin in lung cancer cells, which was abrogated by the knock down of INF2-CAAX (Figure 3I; Figures S3E–S3H). Interestingly, although cortactin and the Arp2/3 complex have also been reported to regulate mtF-actin, knock down of cortactin or inhibition of the Arp2/3 complex with inhibitor had no effect on stress-induced recruitment of fascin to mitochondria (Figures S3I and S3J)

Next, we wished to investigate whether fascin controls mitochondrial OXPHOS through remodeling mtF-actin. The knock down of INF2-CAAX remarkably inhibited mitochondrial OCRs and decreased the levels of NAD+ and NADH in NSCLC cells (Figures S4A–S4C). However, the shRNA depletion of cortactin or inhibition of the Arp2/3 complex with CK666 has no effect on mitochondrial OXPHOS (Figure S4D), suggesting that only ER-originated mtF-actin is required for mitochondrial metabolism. To determine whether INF2-mediated mtF-actin is required for fascin to promote mitochondrial OXPHOS, we knocked down INF2-CAAX in control or fascin-overexpressing NSCLC cells. The knock down of INF2-CAAX in NSCLC cells was able to abrogate the augmentation of mitochondrial OXPHOS in fascin-overexpressing cells, suggesting that ER-originated mtF-actin is required for fascin to promote mitochondrial OXPHOS (Figures 3J and 3K; Figure S4E)

Fascin Regulates the Biogenesis of Respiration Complexes through mtF-Actin

To understand the molecular mechanisms by which fascin regulates mitochondrial OXPHOS, we used tandem mass tag (TMT) and chemical labeling and LC-MS/MS to evaluate the proteomic changes in fascin KO H1650 cells. Over 6,000 proteins were detected and quantified by LC-MS/MS. The expression levels of 76 proteins were differentially expressed ($\log_2$ ratio changes exceeding 2σ away from the mean) in fascin KO cells. Twelve differentially regulated targets are mitochondrial proteins (Figure 4A; Table S2), notably including two subunits of the mitochondrial Complex I (NDUFA4 and NDUFB8) (Figure

4A). Indeed, we confirmed that the protein levels of Complex I subunits NDUFB8, NDUFA4, and mt-ND1 are significantly reduced in fascin KO NSCLC cells (Figures 4B and 4C). Conversely, ectopic expression of wild-type fascin, but not the two bundling defective mutants, was able to increase the levels of mt-ND1 (Figures 4D and 4E). The overexpression of fimbrin had no effect on the expression of mt-ND1 and NDUFB8 (Figure S5A). Disruption of mtF-actin with INF2-CAAX shRNA similarly decreased the protein levels of Complex I subunits (Figure S5B). In contrast, cortactin knock down or Arp2/3 inhibitor treatment had no effect on the Complex I protein level (Figures S5C and S5D). Importantly, the depletion of INF2-CAAX was able to abrogate the fascin-mediated increase in Complex I protein levels (Figures 4F and S5E), suggesting that ER-originated mtF-actin is required for fascin to promote Complex I biogenesis.

It is believed that complexes I, III, and IV are able to assemble into supercomplexes to facilitate electron transfer (Lapuente-Brun et al., 2013). To investigate the regulation of respiratory chain biogenesis by fascin, we determined the levels of respiratory supercomplexes in fascin KO cells. As shown in Figure 4H, Complex I in H1650 cells was almost exclusively present in respirasomes in NSCLC cells (supercomplexes consisting of I, III, and IV). Fascin depletion decreased the levels of respirasomes by about 80% (Figure 4G). Also decreased are supercomplexes III_2+IV_1, III_2, and V_n, while there was little change in the Complex IV monomer (Figure 4G). Interestingly, shRNA knock down of INF2-CAAX similarly reduced the levels of respirasomes and other supercomplexes (Figure 4H), indicating that disruption of mtF-actin is able to recapitulate the effects of fascin depletion. Taken together, our data indicate that fascin controls the biogenesis of respiratory chain by remodeling mtF-actin.

To evaluate the possibility that fascin may regulate respiratory complex biogenesis in lung cancer patients, we used IHC to determine the expression of NDUFB8 in our lung adenocarcinoma tissue microarray (Figure 5A). The overexpression of NDUFB8 in lung adenocarcinoma strongly correlated with poor overall survival (HR = 2.44, p = 0.001), larger tumor size, lymph node metastasis, and advanced TNM (tumor size, lymph node involvement, and distant metastasis) staging (Figure 5B; Table S3), indicating a crucial role for mitochondrial respiration in NSCLC progression. Importantly, lung adenocarcinoma specimens with strong fascin staining also have high NDUFB8 expression (Figures 5C and 5D) (rs = 0.434, p = 0.0025), supporting a role for fascin in the biogenesis of Complex I in lung cancer patients. Taken together, our data supported that fascin promotes the biogenesis of mitochondrial respiratory complexes in NSCLC to augment mitochondrial OXPHOS.

Fascin and mtF-Actin Are Required for the Homeostasis of mtDNA in NSCLC

To investigate the mechanism by which fascin and mtF-actin modulate respiratory chain biogenesis, we determined the protein stability and mRNA transcript levels of nuclear-DNA- and mtDNA-encoded respiratory complex subunits (Figures 6A–6C). Fascin depletion decreased the stability of nuclear-encoded NDUFB8 (Figure 6A) and the mtDNA-encoded mt-ND1 (Figure 6B). Intriguingly, although the RNA transcript levels of mtDNA-encoded genes were significantly decreased after fascin depletion, there was no change in the mRNA levels of nuclear-DNA-encoded Complex I subunits (Figure 6C). The levels of mtDNA and

mtDNA-encoded transcript levels were also remarkably decreased after fascin or INF2-CAAX depletion (Figures S6A–S6C), indicating that fascin and mtF-actin controls biogenesis of respiratory complexes through mtDNA homeostasis. We further investigated the effects of fascin overexpression on mtDNA levels. The overexpression of fascin increased mtDNA levels by approximately 30% in lung cancer cells, which was abrogated by the knock down of INF2-CAAX (Figure S6D), suggesting that fascin controls mtDNA homeostasis through mtF-actin remodeling.

The ER networks are important sensors to cellular stresses, such as unfolded protein response and oxidative stress (Walter and Ron, 2011; Wang and Chan, 2006). In addition, the ER-mitochondrial contact in the proximity of nucleoids is required for mtDNA replication and for the proper segregation of newly replicated mtDNA nucleoids to daughter mitochondria (Friedman and Nunnari, 2014; Lewis et al., 2016; Murley et al., 2013). Because our data support that INF2-CAAX-mediated, ER-originated mtF-actin is required for fascin to promote mitochondrial OXPHOS, we examined the effects of fascin depletion on mtDNA nucleoids by using immunofluorescence staining. mtDNA nucleoids are evenly distributed in the mitochondrial network of control NSCLC cells (Figures 6D and S6E). The depletion of fascin led to striking changes in mtDNA nucleoid morphology and distribution (Figures 6D and S6E). There were long stretches of nucleoid-free mitochondria, aggregation, and enlargement of multiple mtDNA nucleoids in fascin KO H1650 and H23 cells (Figures 6D and S6E). Treatment with DNase I completely abolished the staining of these aggregates, confirming the staining specificity for mtDNA (Figure S6F). Notably, many of the nucleoid aggregates in fascin KO H1650 cells appeared to be on the cytosolic side of the mitochondrial membrane (Figure 6D, arrow), implicating leakage of mtDNA to the cytosol. When quantified by qPCR, the levels of cytosolic mtDNA were two to three times higher in fascin KO cells (Figures 6E and S6G), further supporting the notion of mtDNA leakage after fascin depletion.

To determine the role of fascin-bundling activities in its control of mtDNA homeostasis, we ectopically expressed wild-type fascin or bundling-defective mutants (S39E and 149-151A) in fascin knockdown cells (Figure 6F). Fascin knockdown with shRNA similarly induced mtDNA aggregation in approximately 80% of cells (Figures 6F and S6H). The ectopic expression of wild-type fascin in fascin knockdown cells remarkably prevent mtDNA aggregation (Figures 6F and S6H) and cytosolic mtDNA leakage (Figure 6G). As a consequence, wild-type fascin was also able to restore the levels of mtDNA copies and mtDNA-encoded transcripts in fascin knockdown cells (Figures 6H and 6I). In contrast, the ectopic expression of the two bundling-defective mutants had no rescue effects on mtDNA aggregation and leakage and was not able to restore the levels of mtDNA copies and mtDNA-encoded transcripts (Figures 6F–6I and S6H). Taken together, our data support that fascin controls mtDNA homeostasis through mtF-actin remodeling

The INF2-CAAX and mtF-actin have recently been implicated in the recruitment and activation of Drp1 fission complexes (Hatch et al., 2016; Ji et al., 2015). Therefore, we investigated the role of Drp1 in fascin-mediated mitochondrial OXPHOS. We observed enlarged mtDNA nucleoids in “mito-bulbs” in H1650 cells after Drp1 knock down (Figure S6I), which is consistent with previous observations (Ban-Ishihara et al., 2013). Although

Drp1 knockdown inhibited mitochondrial OXPHOS (Figure S6J), there was no decrease in mtDNA levels or mt-ND1 expression (Figures S6K and S6L). Importantly, Drp1 knockdown had no effect on fascin-mediated increase in Complex I proteins and fascin-mediated augmentation of mitochondrial OXPHOS (Figures S6M and S6N). Taken together, our data suggest that fascin regulates the mtDNA nucleoid homeostasis through mtF-actin-dependent and at least partly Drp1-independent mechanisms. The loss of mtDNA in fascin-depleted cells may result in transcriptional and/or translational downregulation of mtDNA-encoded proteins, which would inhibit the assembly of respiratory complexes and destabilize the nuclear-DNA-encoded respiratory subunits.

Fascin Promotes Metabolic Stress Resistance and Lung Cancer Metastasis by Remodeling mtF-Actin and Augmenting Mitochondrial OXPHOS

To determine the role of mtF-actin in fascin-mediated metabolic stress resistance, we determine the effects of INF2-CAAX knockdown on resistance to glucose limitation and phenformin-induced cell death. As shown in Figures 7A and 7B, fascin promotes cell proliferation and survival under metabolic stresses induced by glucose limitation and phenformin treatment, which was abrogated after depletion of INF2-CAAX, suggesting that mtF-actin is required for fascin-mediated metabolic stress resistance. To investigate the role of mtF-actin in fascin-mediated metastasis, we injected luciferase-labeled H292 cells into nude mice by tail vein and monitored the H292 metastasis through bioluminescence imaging. Although ectopically expressed fascin had only a marginal effect on whole-body photon flux, it markedly increased bioluminescence signals in the head (Figures S7A–S7C), implicating increased brain metastasis in the fascin-overexpression group. *Ex vivo* brain imaging demonstrated that fascin overexpression enhanced H292 metastasis to the brain by 14-fold and remarkably increased the incidence of brain metastasis from 37.5% to 100% (Figures 7C and 7D). The presence of brain metastases in the fascin-over-expression group was also confirmed by H&E staining of the brain sections (Figure S7D). The INF2-CAAX knockdown decreased whole-body photon flux by over 90% (Figure S7A) and abrogated the fascin-mediated increase in brain metastasis (Figures 7C and 7D; Figure S7A), suggesting that mtF-actin is required for fascin to promote lung cancer brain metastasis.

To investigate the role of mitochondrial OXPHOS in fascin-mediated metastasis, we ectopically expressed NDI1, a single-subunit yeast NADH-ubiquinone oxidoreductase, in fascin KO LLC cells. Ectopic NDI1 allows mitochondria to bypass the defective Complex I to use NADH as an electron donor for mitochondrial electron transfer (Figure S7E) (Birsoy et al., 2014; Maas et al., 2010). NDI1 ectopic expression in fascin KO cells was able to rescue reserved-capacity OCRs and remarkably restore the resistance to glucose limitation (Figures S7F and S7G) and metabolic stress-induced cell death (induced by glucose limitation and phenformin) (Figure 7E; Figure S7H) and to rescue anchorage-independent growth (Figure 7F). Fascin KO also remarkably increased both mitochondrial and cytosolic reactive oxygen species (ROS), which could be mitigated by the ectopic expression of NDI1 (Figure S7I), suggesting that fascin might regulate redox balance in lung cancer cells through Complex I regulation. Indeed, supplementation of antioxidant N-acetyl-cysteine (NAC) and (2-(2,2,6,6-Tetramethylpiperidin-1-oxyl-4-ylamino)-2-oxoethyl)triphenylphosphonium chloride (mitoTEMPO) was able to restore the resistance to

phenformin and glucose limitation in fascin KO lung cancer cells (Figures S7J and S7K). To determine the role of mitochondrial OXPHOS in fascin-mediated metastatic colonization, we injected control or fascin KO LLC cells with or without ectopic NDI1 into albino BL6 mice by their tail vein. Fascin depletion in LLC cells abrogated the lung colonization and remarkably prolonged the survival of albino BL6 mice; the ectopically expressed NDI1 in fascin KO LLC cells was able to at least partially restore lung colonization and remarkably shorten survival in mice (Figures 7G and 7H), strongly supporting the notion that fascin controls lung cancer metastasis through augmenting mitochondrial OXPHOS.

DISCUSSION

Here, we report fascin and mtF-actin as regulators of mitochondrial OXPHOS and mtDNA homeostasis in lung cancer. The depletion of fascin destabilizes mtF-actin and interferes with mtDNA maintenance, which results in mtDNA loss. mtDNA encodes essential subunits of respiratory complexes I, III, IV, and V and two mitochondrial ribosomal RNAs. The loss of mtDNA in fascin-depleted lung cancer cells resulted in the inhibition of respiratory complex biogenesis and metabolic stress resistance. By promoting mitochondrial OXPHOS and metabolic stress resistance, fascin promotes metastatic expansion. Taken together, our data support that fascin plays a metabolic role in the metastatic colonization of NSCLC (Figure S7L).

The regulation of mitochondrial metabolism and mtDNA homeostasis by fascin and mtF-actin appears to be partly through mechanisms distinctly different from Drp1-mediated mitochondrial fission. A previous report suggested that β-actin and myosin II were integral components of mtDNA nucleoids (Reyes et al., 2011). However, our data and that of others indicate that fascin and mtF-actin are at the cytosolic side of the mitochondrial outer membrane (Ji et al., 2015; Korobova et al., 2013; Manor et al., 2015). Intriguingly, although cortactin and the Arp2/3 complex have also been reported to promote mtF-actin assembly, inhibition of these two proteins has no effect on the mitochondrial recruitment of fascin. One possibility is that cortactin and the Arp2/3 complex facilitate the polymerization of dendritic actin networks, which is not compatible with fascin-mediated bundling of parallel actin filaments. The inhibition of Arp2/3 or depletion of cortactin also had no effects on mitochondrial OXPHOS or the biogenesis of respiratory Complex I, suggesting that the regulation of mitochondrial metabolism is specific to INF2-CAAX-mediated, ER-originated mtF-actin. The ER network is responsible for important cellular stress responses (Walter and Ron, 2011; Wang and Chan, 2006). There is recent evidence that the ER-mitochondrial contacts are required for initiating mtDNA replication (Lewis et al., 2016). It is possible that fascin and mtF-actin modulate the mtDNA homeostasis and augment mitochondrial metabolism through the ER-mitochondrial crosstalk.

Our data indicate that fascin is able to regulate mitochondrial metabolism and metastatic expansion in NSCLC by remodeling mtF-actin. Although the dysregulated actin cytoskeleton in cancer cells has been extensively studied in the context of metastatic dissemination, the post-dissemination role of the actin cytoskeleton in metastatic progression is unclear. Our findings in NSCLC models suggest that the rearrangement of the actin

cytoskeleton in metastatic cancer cells is able to reprogram mitochondrial metabolism to promote the survival and metastatic expansion of disseminated cancer cells.

Fascin expression is absent in most adult epithelial cells (including lung epithelial cells) (Hashimoto et al., 2005), suggesting that it is optional for the normal physiology and metabolism in non-transformed epithelia. Intriguingly, metastatic cancer cells dramatically increase fascin expression, possibility in response to the inflammatory and hypoxic tumor microenvironment (Snyder et al., 2011; Sun et al., 2011; Zhao et al., 2014). Our data indicate that fascin confers a survival advantage to cancer cells in the nutrient-deprived tumor environment by augmenting mitochondrial metabolism and metabolic stress resistance. On the other hand, lung cancer overexpressing fascin might also become addicted to fascin-mediated mitochondrial metabolism through non-oncogene addictions (Luo et al., 2009), which likely creates a therapeutic vulnerability that could be exploited to prevent metastatic recurrence in fascin-overexpressing lung cancer.

Taken together, our studies revealed an unexpected role of fascin in the metastatic colonization of NSCLC by augmenting mitochondrial OXPHOS. However, there are a few outstanding questions and limitations that remain to be addressed in the future. First, although our data demonstrate that fascin regulates mitochondrial metabolism in lung adenocarcinoma, it is still unclear whether such findings could be extrapolated to other cancer types. Second, the role of mitochondria in tumor initiation, metastasis, and progression appeared to be dependent on tumor histology and stage. For example, there was evidence in colorectal cancer, breast cancer, and melanoma that mild inhibition of mitochondrial OXPHOS promotes tumor initiation and metastasis (Porporato et al., 2014; Woo et al., 2012). In a recent study, Reznik et al. (2016) surveyed the changes in mtDNA copy number across 15 different types of cancer (relative to paired normal tissue) and discovered that lung adenocarcinoma was the only cancer type with increased mtDNA copies in cancer tissues. The elevated mitochondrial OXPHOS in lung adenocarcinoma could be in part due to genetic disruption of the switch/sucrose non-fermentable (SWI/SNF) complex (Lissanu Deribe et al., 2018), which promotes lung cancer tumor growth and progression. Third, this study used a tail-vein injection model to study the mitochondrial role of fascin in metastatic colonization and expansion. Although the choice of this experimental approach is oriented toward investigating the post-dissemination role of fascin in lung cancer metastasis, it would not be able to address the mitochondrial role of fascin in tumor cell migration, invasion, and metastatic dissemination. Interestingly, there is evidence that mitochondrial dynamics could have critical roles in cell migration and invasion (Zhao et al., 2013). Therefore, future investigation using orthotopic metastasis models and cell migration and invasion assays is warranted.

STAR★METHODS

LEAD CONTACT AND MATERIALS AVAILABILITY

Further information and requests for resources and reagents should be directed to and will be fulfilled by the Lead Contact, Shengyu Yang (sxy@psu.edu). Plasmids generated in this study will be available upon request with Material Transfer Agreements.

EXPERIMENTAL MODEL AND SUBJECT DETAILS

Cell culture—The lung cancer cell lines (H1650, H23, H292 and LLC) were obtained from the ATCC and Moffitt Cancer Center Lung Cancer Center of Excellence cell line repository and authenticated using Short Tandem Repeat profiling. All cell lines used were free of microbial (including mycoplasma) contamination. H1650, H23, H292 were cultured in RPMI medium supplemented with 10% fetal bovine serum and 1% Penicillin-Streptomycin. LLC was cultured in DMEM medium supplemented with 10% fetal bovine serum and 1% Penicillin-Streptomycin. All the cells were maintained at 37°C in a humidified 5% CO_2 incubator.

CRISPR/Cas9 knockout in lung cancer cells—Fascin knock out was performed using pLenti CRISPR V2 vector (Addgene_52961) (Sanjana et al., 2014) encoding sgRNA targeting Fascin (human Fascin: sgRNA, GAAGAAGCAGATCTGGACGC; mouse Fascin: sgRNA, TCGCTACCTGGCCGCCGACA). To generate stable fascin knockout lung cancer cells, cells were infected with control or sgRNA encoding lentiviral vectors, selected with puromycin and pooled together after drug selection. The depletion of fascin in the cells were confirmed using western blotting.

Inducible Cas9 knockout of fascin in LLC cells—LLC cells were infected with pLenti CMVtight -Cas9 Hygro and pLenti CMV rtTA3 Blast (w756-1) (Addgene_26429) and selected with hygromycin and blasticidin. Single clones were induced with 1 μg/ml doxycycline for 3 days and stained with anti-Flag antibody to examine the expression levels of Tet-On Flag-Cas9. 15 clones with high Cas9 expression were combined, infected with pLentiGuide.Puro selected with puromycin. The cells were then treated with 1ug/ml doxycycline for 7 days, and the expression of Flag-Cas9 and deletion of fascin were examined by western blotting.

Animal models—All animal experiments were performed following the NIH guidelines and according to protocols approved by the Moffitt Cancer Center IACUC or the Penn State College of Medicine IACUC. 6-7 weeks old NCr nu/nu mice (male or female) and Albion BL6 mice (female) were purchased from Charles Rivers and used in this study. Mice are housed in a pathogen-free facility and kept in a temperature-controlled room set to a light and dark cycle of 12 hours each. For the treatment studies mice were randomly assigned to different treatment group.

Human tissue samples—A total of 113 sequential lung adenocarcinoma tumor tissues were collected from patients who had received radical surgery at Tianjin Medical University Cancer Institute and Hospital (TJMUCH). Retrospective clinicopathological data of these patients, including age, sex, tumor size, regional lymph node status, TNM stage, pathologic type and survival data, were also obtained. These formaldehydefixed paraffin-embedded tissues were constructed into tissue microarrays for further immunohistochemistry analysis. Another set of 82 pairs of lung adenocarcinoma tumor tissues and corresponding adjacent non-tumor tissues were collected and sectioned to analyze the differential expression levels of fascin. The usage of these specimens and the patient information were approved by the Ethics Committee of TJMUCH. All patients provided written consent for the use of their

specimens and disease information for future investigations according to the ethics committee. The age, and sex of the subjects is provided in Tables S1 and S3. Sample size information is indicated in the figure legends.

METHOD DETAILS

cDNA constructs—To rescue Fascin knockdown or overexpress Fascin proteins, wild-type or mutant Fascin (S39E and 149-151A mutants) (Yang et al., 2013) cDNAs were subcloned into pLenti.CMV.blasticidin vector (Addgene_17486) (Campeau et al., 2009) between BamH I and XhoI sites. The inducible Cas9 construct was generated by inserting hSpCas9 PCR product (using pX330-U6-Chimeric_BB-CBh-hSpCas9 as template) (Cong et al., 2013) into pENTR TOPO® vector. The pENTR-Cas9 and pLenti CMVtight -DEST (Addgene_26433) was then used for the construction of pLenti CMVtight -Cas9 Hygro through LR recombination. pLNCX2-mApple-Lifeact has been previously reported (Sun et al., 2014) and deposited to Addgene_89820.

Drug treatment—To induce mtF-actin accumulation and EGFP-fascin recruitment to mitochondria, cells were incubated with 5 μM FCCP in cell culture medium (37°C, 5% CO2 for 60 minutes) or cultured in cell culture medium containing 1mM Glc (37°C, 5% CO2, for overnight) before being used for immunofluorescence staining. To inhibit protein translaction, cells were treated with doxycycline (10μg/ml) or cyclo-heximide (50 μg/ml) in cell culture medium for various time as indicated before being lysed for western blotting. To inhibit Arp 2/3 complex, cells were treated with 50 μM CK-666 for 24h (for western blotting) or overnight (for fluorescence imaging).

RNA interference—The knockdowns of Fascin and INF2-CAAX were achieved using pSUPER.Retro.puro vector (Oligoengine) encoding shRNA targeting mouse/human Fascin (Sun et al., 2011, 2013), human Cortactin, and human INF2-CAAX (Korobova et al., 2013). To rescue Fascin knockdown or overexpress Fascin proteins, wild-type or mutant Fascin (S39E and 149-151A mutants) (Yang et al., 2013) cDNAs were subcloned into pLenti.CMV.blasticidin vector (Addgene_17486) (Campeau et al., 2009). pLKO vector encoding shRNAs for DRP1 were purchased from Sigma (sh1 TRCN0000318424; sh2 TRCN0000318425). The retroviral and lentiviral particles were packaged in HEK293 cells using the PEI transfection method, and concentrated as previously described (Yang et al., 2012).

Western blotting—Cells were lysed in SDS-NP40 buffer (50 mM Tris, pH 8.0, 150 mM NaCl, 1% NP40,1% SDS, 1mM protease inhibitors cocktail) on ice for 1 min. Cells were scraped from the plate and sonicated briefly three times. Then lysates were heated at 95°C for 5 min and centrifuged at 20,000 × g at 4°C for 10 min. To prepare cell lysate for detection of protein phosphorylation, cells were lysed in Triton x-100 buffer (50 mM Tris, pH 7.4, 150 mM NaCl, 1% Triton x-100, 1 mM EDTA, 1mM phosphatase inhibitor cocktail (Thermo Scientific, Cat#88667), 1 mM protease inhibitors cocktail (Roche, Cat# 04693159001)) on ice for 15 min. The protein concentrations of the cell lysates were determined using BCA method (Thermo Scientific Pierce, Cat# PI-23225). 50 μg Proteins were separated by SDS-PAGE and transferred onto PVDF membrane. The membranes were

incubated in blocking buffer (5% (w/v) nonfat dry milk in Tris-buffered saline, 0.05% Tween 20 (TBS-T)) for 30 min at RT., and incubated with primary antibodies for 16 h at 4°C, followed by incubation with secondary antibodies for 60 min at RT.

Immunofluorescence staining and microscopy—Immunofluorescence staining were carried out as previously described (Sun et al., 2014) with modifications. 80,000 cells were seeded onto laminin coated coverslips in 12-well plates overnight. Cells were then fixed with 4% fresh paraformaldehyde in phosphate buffered saline (PBS) at room temperature (RT) for 20 min. Cells were then incubated with primary antibodies (Alexa Fluor® 555 Mouse anti-Cytochrome C or rabbit anti-TOM20 for mitochondrial staining, mouse anti-DNA antibody, clone AC-30-10 for mtDNA nucleoid staining) diluted in antibody dilution buffer (2% BSA 0.1% Triton X-100 in TBS) for 60 min at RT. When F-actin staining was needed, Alexa Fluor 488 phalloidin (0.4 unit/ml) was included in the primary antibody solutions. Cells were then incubated with secondary antibodies for 60 min at RT and then with DAPI at RT for 10 min. Extensive washing with TBS was performed between each step. After a final wash with TBS the coverslips were mounted with Fluoromount (Sigma).

For Fascin staining, cells were fixed with cold (−20°C) methanol and incubated at −20°C for 20 min. After fixation, cells were rehydrated with 2% BSA 0.1% Triton X-100 in TBS for at RT for 20 min and then incubated with anti-Fascin and anti-TOM20 antibodies at 4°C for overnight. For EGFP-Fascin imaging, H23 cells were infected with pLNCX2-EGFP-Fascin1 retrovirus and pLV-mitoDsRed (Addgene_44386) lentivirus. 48 hours after infection, cells were imaged using Leica DMI8 TCS SP8 confocal microscope.

For wide-field fluorescence microscopy, samples were examined with an automated upright microscope (Axiovert S100) through a 63 × /1.3 FLUAR Plan Apochromatic oil immersion objective. Images were captured using the charge-coupled device camera (Axiocam 503 mono) and ZEN 2.3 blue edition (Zeiss). For confocal microscopy, samples were viewed with an inverted microscope (DMI8; Leica), confocal scanner (TCS SP8; Leica), and a HC PL APO 63 × /1.4 CS2 oil immersion objective (Leica). 488 and 552 STED laser lines were applied to excite the samples, and a tunable acousto-optical beam splitter was used to minimize crosstalk between fluorochromes. Gain, offset, pinhole, and lookup table settings were identical for all samples. Images were captured with photomultiplier detectors and prepared with the Leica Application Suite X (Leica).

Immunohistochemistry (IHC)—IHC staining was used to determine Fascin and NDUFB8 expression levels in tumor tissues and non-tumor tissues. Briefly, paraffin-embedded sections of tissues were deparaffinised and then heated in a pressure pot for 3 minutes to retrieve the antigens. The slides sections were then incubated with primary antibodies (1:200) overnight at 4°C. Antibody binding was detected using a peroxidase–conjugated secondary antibody at 37°C for 30 minutes. A DAB Substrate Kit was used to perform the chromogenic reaction. The intensity of the staining was evaluated by two independent investigators blinded to the clinicopathological data of patients using the following criteria: 0, negative; 1, low; 2, medium; 3, high. The extent of staining was scored as 0, 0% stained; 1, 1% to 25% stained; 2, 26% to 50% stained; 3, 51% to 100% stained. Five random fields (20 × magnification) were evaluated under a light microscope. The final

scores were calculated by multiplying the scores of the intensity with those of the extent and dividing the samples into four grades: 0, negative (−); 1 to 2, low staining (+); 3 to 5, medium staining (++); 6 to 9, high staining (+++).

Mitochondrial isolation—All the mitochondrial isolation steps were carried out at 4°C or on ice. 5×10^6 cells were harvested by scraping, washed once with mitochondrial isolation buffer (MIB, 200 mM sucrose, 10 mM Tris, 1 mM EGTA, using HEPES-KOH to adjust to pH 7.5. Fresh 1X protease inhibitor cocktail was added prior to for mitochondrial isolation). Cells were resuspended in 1ml MIB, and passed through 27G needle 30-35 times to break the cells. The cell lysate were then centrifuged at 500 × g for 10min. The supernatant was transferred to a new tube and then centrifuged at 7,000 × g for 10min. The mitochondria in the pellet were washed once with MIB and centrifuged at 10,000 × g for another 10min. The pellet was then resuspended in 300 μl MIB and the amount of mitochondrial protein was determined using BCA method.

Blue native electrophoresis and immunoblot—Blue native (BN) electrophoresis was performed at 4°C using NativePAGETM precast gel (Thermo Scientific, Cat# BN1001BOX) as previously described (Jha et al., 2016) with modifications. The BN sample buffer (BNSB, 5 μl native sample buffer, 8 μl digitonin, 7 μl sterilized water, for 50 μg mitochondria protein) were prepared using the NativePAGE Sample Prep Kit (Thermo Scientific, Cat#BN2008). The BNSB was added to 50 μg of mitochondria pellet and mixed gently to avoid bubble formation. The mixture was incubated on ice for 30 min and then centrifuged at 20,000 × g at 4°C for 10 min. 20 μl supernatant was mixed with 2 μl Coomassie Brilliant Blue G-250 from the kit and loaded to the NativePAGETM gel (3%–12% Bis-Tris gel). The anode buffer (1x NativePAGETM running buffer) and cathode buffer A (anode buffer + 0.2g/L Coomassie Brilliant Blue G-250) were prepared from 20x NativePAGETM running buffer (Thermo Scientific, BN2001). After electrophoresis at 150 V, 4°C for 45 min, the cathode buffer A was replaced with cathode buffer B (cathode buffer A mixed with anode buffer at a ratio of 1:10) and continued at 250 V, 4° C for 90 min. The gel was then washed with transfer buffer (TB, 1 × NuPAGETM transfer buffer, Thermo Scientific, Cat# NP00061, plus 10% methanol) for 3 times and then incubated with TB for 20 min at RT with shaking. The proteins on the gel were transferred to PVDF membrane using conventional western blotting transfer device (300 mA, 120 min, on ice). After the transfer was complete, the PVDF membrane was fixed with 10% acetic acid immediately for 10 min on a shaker. The membrane was then washed with deionized water (DDW) for 5 times (3 min each) and air-dried completely. The air-dried membrane was then washed with methanol for 5 times (3 min each), and then with DDW for 5 times (3 min each) and then subjected to western blotting using anti-OXPHOS antibody cocktail (Thermo Scientific, Cat# 45-7999) plus anti-mtCO1 antibody (Fisher Scientific, Cat# 43-9800), or antibodies for respective respiration complexes.

Mitochondrial stress test—Oxygen consumption rate (OCR) was determined with a Seahorse XF96 Extracellular Flux Analyzer (Agilent Seahorse Bioscience) following protocols recommended by the manufacturer. Cells were seeded on XF96 microplates (10,000 cells/well). Cells were maintained in a non-buffered assay medium (Agilent) in a

non-CO2 incubator for 30 min before the assay. The XF Cell Mito Stress Test Kit (Agilent), was used for the assay. The baseline recordings were followed by sequential injection of 1 μM oligomycin, 1 μM FCCP, and 1 μM rotenone/ 20 μM antimycin A.

NAD+ and NADH quantification—The levels of NAD+ and NADH were determined using the NAD+ /NADH assay kit from Biovision (Cat# k337-100). Approximately 200,000 cells were harvested and extract by 2x freeze/ thaw cycles in 400 μl Extraction Buffer. The extraction were centrifuged at 20,000 × g at 4°C for 5 min, and the supernatant was used to determine total NAD (NADt, NADH and NAD) and NADH according to the manufacturer's instruction.

Soft agar assay—Each 12-well plate was coated with 1 mL of bottom agar (prepared with RPMI/DMEM medium supplemented with 10% FBS and 0.75% low melting agar (Fisher Scientific, Cat# BP165-25) and allowed to solidify. 3,000 cells were suspended in 1 mL top agar (RPMI/DMEM containing 10% FBS and 0.375% low melting agar) and seeded to each well. 1ml RPMI/DMEM complete medium were added to the well after the top agar solidified. The medium were replaced every three days. After 14-21 days, the colonies were stained with iodonitrotetrazolium chloride (Biosynth, Cat# I-7630) overnight to visualize colony formation, and the number of colonies per well were quantified using ImageJ software.

Cell proliferation assay—Cells were seeded at 80,000/ well in a 6-well plate in triplicate in RPMI complete medium containing 10 mM or 1 mM glucose. The cell culture media were changed every day. Cells were fixed with 10% formalin for 20min and stained with 100 μl crystal violet solution (Eng Scientific, Cat# INC NO. 6100) for 20 min with shaking. After washing, the crystal violet staining was solubilized with 1 mL 10% acetic acid and absorbance at OD 590 nm was measured.

Cell phenformin sensitivity assay—60,000 cells were seeded to 12 wells plate in RPMI medium containing 1 mM glucose and phenformin before being subjected to Propidium iodide (PI) staining to evaluate cell death. The phenformin treatment concentrations and times varied depending on cell lines and experimental conditions: H292 cells were treated with 40 μM phenformin for 48 h; LLC cells were treated with 20 μM phenformin for 24 h; H1650 and H23 cells were treated with 40 μM (for fascin depletion experiments), 100 μM (for H1650 fascin overexpression experiment) or 200 μM (for H23 fascin overexpression experiment) phenformin for 48 h.

RNA isolation and qPCR—1×10^6 cells were washed with ice-cold PBS and total RNA was extracted using RNeasy Kit (QIAGEN Cat# 74106). 1 μg RNA was used for the reverse transcription. cDNAwas diluted 1:10 then used for qPCR with ABI qPCR master mix (Thermo, Cat# 4367659).

Quantitation of cytosolic mtDNA—The cytosolic mtDNA was quantified as previously described (West et al., 2015). 2×10^6 cells were each divided into two equal aliquots, and one aliquot was used for total DNA extraction using DNeasy Kit (QIAGEN, Cat# 69504). The second aliquots were resuspended in 500 μl buffer (150 mM NaCl, 50 mM HEPES, and

25 μl /ml digitonin (EMD), pH 7.5) and incubated on ice for 10 min to permeabilize the plasma membrane. The cell lysate were then centrifuged at 1000 × g, 5 min 3 times at 4°C. The supernatant was transferred to a new tube and centrifuge at 20000 × g for 10 min at 4°C. The cytosolic DNA in the supernatant was extracted using DNeasy Kit. Quantitative PCR was performed using DNA extracted from both whole-cell extracts and cytosolic fractions using nuclear DNA primers and mtDNA primers in Table S3.

Lewis Lung Cancer (LLC) cell lung extravasation pilot experiment—5×10^5 mApple-Lifeact labeled LLC cells were suspended in 300 μl DMEM base medium and injected via tail vein into 7 week-old BL6 female mice. 2, 24 h, or 48 h after LLC cell injection, mice were tail-vein injected with 100 μl DyLight 488 Lycopersicon Esculentum Lectin (1mg/ml) (Vector Laboratories, Cat#DL-1174) to label vascular endothelial cell marker. The mice are euthanized and the lungs were extracted for extra vital imaging using FV1000 MPE Multiphoton Laser Scanning Microscope (Olympus) and 60 × /0.9 LUM Plan FI/IR water immersion objective was used for imaging. Multi-line Argon 488 nm and Green HeNe 543 nm STED laser lines were applied to excite the samples, and a tunable acousto-optical beam splitter was used to minimize crosstalk between fluorochromes. Images were captured with photomultiplier detectors and prepared with FV10-ASW (Olympus).

Metastatic colonization

For H292 lung colonization experiments, nude mice were randomly assigned to two groups (8 mice each, female). 5×10^6 luciferase labeled H292 cells were resuspended in 300 μl DMEM medium (serum free) and inoculated into 7 week-old female nude mice via tailvein. Noninvasive bioluminescent imaging by injecting specimen intra-peritoneal (i.p.) with 10 minutes prior to imaging with 150mg/kg of D-luciferin in DPBS, and analysis were performed as described previously with Xenogen IVIS 200 (8).

For LLC metastatic expansion experiment, 5×10^5 luciferase labeled LLC cells stabling expressing Tet-On Cas9 and Fascin sgRNA were resuspended in in 300 μl DMEM medium (serum free) and tail-vein injected into 7 week-old Albino BL6 female mice. The mice were randomly assigned to two groups (10 mice each). One group was provided with doxycycline chow (BioServ, Cat# S3888) 48 h after tail vein injection; the other group was continued with regular chow. Bioluminescence imaging was performed as indicated to monitor metastatic expansion of disseminated LLC cells. For pharmacological inhibition of Fascin, mice were randomly assigned to two groups (10 mice each, female).48 hours after tail-vein injection. Mice were administered daily with 100mg / kg G2 (Enamine, Cat# EN300-246105) via i.p. or with vehicle control.

For H292 brain metastasis experiment, nude mice were randomly assigned to four groups (8 mice each, male), 5×10^6 luciferase labeled H292 cells with or without Fascin overexpression or INF2-CAAX knockdown were injected via tail. To image brain metastasis, mice were i.p. injected with 150mg / kg D-luciferin and euthanized after 5 minutes. The brain was carefully extracted within 3 minutes and soaked 500 μl D-luciferin (15 mg / ml) solution at 37°C for 10 minutes before bioluminescence imaging.

For NDI1 rescue experiment, 5×10^5 luciferase labeled LLC cells with or without Fascin knockout or NDI1 overexpression were tail-vein injected into Albino BL6 female mice. Bioluminescence imaging was performed as indicated to monitor metastatic colonization by disseminated LLC cells.

Metabolomics and metabolic flux analysis—Control or Fascin knockout H1650 cells were extracted with 80% methanol and metabolite extracts were analyzed through LC-MS/MS for relative metabolite changes using Selected Reaction Monitoring (SRM) method. About 280 polar metabolites encompassing different metabolic pathways including glycolysis, TCA cycle, nicotinamide metabolism, amino acid metabolism etc. were analyzed using Acquity UPLC and Xevo TQS (Waters) based platform (Shukla et al., 2017). Peak areas were normalized with the respective protein concentrations and the resultant peak areas were subjected to metabolomic analyses by utilizing Metaboanalyst 2.0. Relative difference in metabolite levels were compared using Student's t test.

For metabolic flux analysis, 1×10^7 H1650 cells were incubated with RPMI medium containing 10 mM [U-13C] Glucose for 6 hours. After washing with PBS once, the cells were extracted using 4 mL of cold (−20°C) 70% methanol and incubated in −80°C for 10 minutes. The labeled and unlabeled metabolites were analyzed through LC-MS using Thermos Exactive Plus Orbitrap Mass Spectrometer. Peak areas were normalized with the respective protein concentrations and the resultant peak areas were analyzed using MSDIAL 3.2.

Proteomics—To compare protein expression levels in control and Fascin KO cells, chemical labeling using tandem mass tags (TMT) was combined with liquid chromatography-tandem mass spectrometry discovery proteomics. Samples were prepared in biological duplicate. Protein lysates were made using aqueous denaturing buffer containing 20 mM HEPES and 8 M urea, prior to reduction of disulfides, alkylation of cysteines, and tryptic digestion (Worthington). The resulting peptides are extracted using C-18 Sep-Pak cartridges, dried, and resuspended in 100 mM aqueous triethylammonium bromide (TEAB) for TMT labeling. Each channel is analyzed with LC-MS/MS for quality control (i.e., tag incorporation and reporter ion verification). Then, samples are mixed using equal amounts of total protein and fractionated with basic pH reversed phase liquid chromatography; each peptide fraction is analyzed in duplicate with LC-MS/MS (RSLCnano and QExactive Plus, Thermo). Data are analyzed with MaxQuant (Cox and Mann, 2008), which identifies each peptide using sequence specific ions and quantifies relative expression level in each sample using the TMT Reporter ions. After iterative rank order normalization to correct for differences in loading, significant differences were determined as proteins that exceeded 2 times the standard deviation away from the mean log2 ratio between the two samples (Welsh et al., 2013).

QUANTIFICATION AND STATISTICAL ANALYSIS

All data are shown as mean values ± standard deviation (SD) unless indicated otherwise. Sample numbers of data obtained from animal experiments refer to the number of individual mice, as specified in the figure legends. Experiments on cultured cells were performed using

at least 3 independent biological replicates. Log-rank tests were used for survival analysis. Categorical data were analyzed using Fisher's exact test or Chi-square test. Spearman's rank-order correlation was used to determine the correlation between immunohistochemistry staining intensities for different antigens. Comparison of two independent groups was performed with unpaired two-tailed Student's t test. No samples, data points, or animals were excluded from the analysis. Statistical analysis were performed using GraphPad Prism 7 or SPSS software.

DATA AND CODE AVAILABILITY

The mass spectrometry proteomics data have been deposited to the ProteomeXchange Consortium via the PRIDE partner repository with the dataset identifier PXD014753 and 10.6019/PXD014753. Metabolomics data are available upon request.

Supplementary Material

Refer to Web version on PubMed Central for supplementary material.

ACKNOWLEDGMENTS

This work is supported, in part, by grants from the NIH (R01CA175741 and R01CA233844 to S.Y. and R01CA210439 and R01CA216853 to P.K.S.) and the Elsa U. Pardee Foundation (to S.Y.). Proteomics is supported, in part, by the National Cancer Institute through a Moffitt's Cancer Center support grant (P30-CA076292) and the Moffitt Foundation. We would also like to acknowledge the Fred & Pamela Buffett Cancer Center support grant (P30CA036727, NCI) for supporting shared resources. We thank Drs. J. Cleveland, H.-G. Wang, K. Aird, and H. Higgs for advice and discussions.

REFERENCES

Ban-Ishihara R, Ishihara T, Sasaki N, Mihara K, and Ishihara N (2013). Dynamics of nucleoid structure regulated by mitochondrial fission contributes to cristae reformation and release of cytochrome c. Proc. Natl. Acad. Sci. USA 110,11863–11868. [PubMed: 23821750]

Barnawi R, Al-Khaldi S, Majed Sleiman G, Sarkar A, Al-Dhfyan A, Al-Mohanna F, Ghebeh H, and Al-Alwan M (2016). Fascin Is Critical for the Maintenance of Breast Cancer Stem Cell Pool Predominantly via the Activation of the Notch Self-Renewal Pathway. Stem Cells 34, 2799–2813. [PubMed: 27502039]

Birsoy K, Possemato R, Lorbeer FK, Bayraktar EC, Thiru P, Yucel B, Wang T, Chen WW, Clish CB, and Sabatini DM (2014). Metabolic determinants of cancer cell sensitivity to glucose limitation and biguanides. Nature 508, 108–112. [PubMed: 24670634]

Birsoy K, Wang T, Chen WW, Freinkman E, Abu-Remaileh M, and Sabatini DM (2015). An Essential Role of the Mitochondrial Electron Transport Chain in Cell Proliferation Is to Enable Aspartate Synthesis. Cell 162,540–551. [PubMed: 26232224]

Campeau E, Ruhl VE, Rodier F, Smith CL, Rahmberg BL, Fuss JO, Campisi J, Yaswen P, Cooper PK, and Kaufman PD (2009). A versatile viral system for expression and depletion of proteins in mammalian cells. PLoS One 4, e6529. [PubMed: 19657394]

Chen L, Yang S, Jakoncic J, Zhang JJ, and Huang XY (2010). Migrastatin analogues target fascin to block tumour metastasis. Nature 464, 1062–1066. [PubMed: 20393565]

Cong L, Ran FA, Cox D, Lin S, Barretto R, Habib N, Hsu PD, Wu X, Jiang W, Marraffini LA, et al. (2013). Multiplex genome engineering using CRISPR/Cas9 systems. Science 339, 819–823. [PubMed: 23287718]

Cox J, and Mann M (2008). MaxQuant enables high peptide identification rates, individualized p.p.b.-range mass accuracies and proteome-wide protein quantification. Nat. Biotechnol. 26, 1367–1372. [PubMed: 19029910]

De Vos KJ, Allan VJ, Grierson AJ, and Sheetz MP (2005). Mitochondrial function and actin regulate dynamin-related protein 1-dependent mitochondrial fission. Curr. Biol. 15, 678–683. [PubMed: 15823542]

Friedman JR, and Nunnari J (2014). Mitochondrial form and function. Nature 505, 335–343. [PubMed: 24429632]

Friedman JR, Lackner LL, West M, DiBenedetto JR, Nunnari J, and Voeltz GK (2011). ER tubules mark sites of mitochondrial division. Science 334, 358–362. [PubMed: 21885730]

Hashimoto Y, Skacel M, and Adams JC (2005). Roles of fascin in human carcinoma motility and signaling: prospects for a novel biomarker? Int. J. Biochem. Cell Biol. 37, 1787–1804.

Hatch AL, Ji WK, Merrill RA, Strack S, and Higgs HN (2016). Actin filaments as dynamic reservoirs for Drp1 recruitment. Mol. Biol. Cell 27, 3109–3121. [PubMed: 27559132]

Huang FK, Han S, Xing B, Huang J, Liu B, Bordeleau F, Reinhart-King CA, Zhang JJ, and Huang XY (2015). Targeted inhibition of fascin function blocks tumour invasion and metastatic colonization. Nat. Commun. 6, 7465. [PubMed: 26081695]

Jha P, Wang X, and Auwerx J (2016). Analysis of mitochondrial respiratory chain supercomplexes using blue native polyacrylamide gel electrophoresis (BN-PAGE). Curr. Protoc. Mouse Biol. 6, 1–14. [PubMed: 26928661]

Ji WK, Hatch AL, Merrill RA, Strack S, and Higgs HN (2015). Actin fil-amentstarget the oligomeric maturation of the dynamin GTPase Drp1 to mitochondrial fission sites. eLife 4, e11553. [PubMed: 26609810]

Kitay BM, McCormack R, Wang Y, Tsoulfas P, and Zhai RG (2013). Mislocalization of neuronal mitochondria reveals regulation of Wallerian degeneration and NMNAT/WLD(S)-mediated axon protection independent of axonal mitochondria. Hum. Mol. Genet. 22, 1601–1614. [PubMed: 23314018]

Korobova F, Ramabhadran V, and Higgs HN (2013). An actin-dependent step in mitochondrial fission mediated by the ER-associated formin INF2. Science 339, 464–467. [PubMed: 23349293]

Korobova F, Gauvin TJ, and Higgs HN (2014). A role for myosin II in mammalian mitochondrial fission. Curr. Biol. 24, 409–414. [PubMed: 24485837]

Lapuente-Brun E, Moreno-Loshuertos R, Acín-Pérez R, Latorre-Pellicer A, Colás C, Balsa E, Perales-Clemente E, Quirós PM, Calvo E, Rodríguez-Hernández MA, et al. (2013). Supercomplex assembly determines electron flux in the mitochondrial electron transport chain. Science 340, 1567–1570. [PubMed: 23812712]

Lewis SC, Uchiyama LF, and Nunnari J (2016). ER-mitochondria contacts couple mtDNA synthesis with mitochondrial division in human cells. Science 353, aaf5549. [PubMed: 27418514]

Li A, Morton JP, Ma Y, Karim SA, Zhou Y, Faller WJ, Woodham EF, Morris HT, Stevenson RP, Juin A, et al. (2014). Fascin is regulated by slug, promotes progression of pancreatic cancer in mice, and is associated with patient outcomes. Gastroenterology 146, 1386–1396.e17. [PubMed: 24462734]

Li S, Xu S, Roelofs BA, Boyman L, Lederer WJ, Sesaki H, and Karbowski M (2015). Transient assembly of F-actin on the outer mitochondrial membrane contributes to mitochondrial fission. J. Cell Biol. 208, 109–123. [PubMed: 25547155]

Lin S, Lu S, Mulaj M, Fang B, Keeley T, Wan L, Hao J, Muschol M, Sun J, and Yang S (2016). Monoubiquitination Inhibits the Actin Bundling Activity of Fascin. J. Biol. Chem. 291, 27323–27333. [PubMed: 27879315]

Lissanu Deribe Y, Sun Y, Terranova C, Khan F, Martinez-Ledesma J, Gay J, Gao G, Mullinax RA, Khor T, Feng N, et al. (2018). Mutations in the SWI/SNF complex induce a targetable dependence on oxidative phosphorylation in lung cancer. Nat. Med. 24, 1047–1057. [PubMed: 29892061]

Liu X, Romero IL, Litchfield LM, Lengyel E, and Locasale JW (2016). Metformin Targets Central Carbon Metabolism and Reveals Mitochondrial Requirements in Human Cancers. Cell Metab. 24, 728–739. [PubMed: 27746051]

Luo J, Solimini NL, and Elledge SJ (2009). Principles of cancer therapy: oncogene and non-oncogene addiction. Cell 136, 823–837. [PubMed: 19269363]

Maas MF, Sellem CH, Krause F, Dencher NA, and Sainsard-Chanet A (2010). Molecular gene therapy: overexpression of the alternative NADH dehydrogenase NDI1 restores overall physiology in a fungal model of respiratory complex I deficiency. J. Mol. Biol. 399, 31–40. [PubMed: 20398675]

Manor U, Bartholomew S, Golani G, Christenson E, Kozlov M, Higgs H, Spudich J, and Lippincott-Schwartz J (2015). A mitochondria-anchored isoform of the actin-nucleating spire protein regulates mitochondrial division. eLife 4, e08828.

Murley A, Lackner LL, Osman C, West M, Voeltz GK, Walter P, and Nunnari J (2013). ER-associated mitochondrial division links the distribution of mitochondria and mitochondrial DNA in yeast. eLife 2, e00422. [PubMed: 23682313]

Pelosi G, Pastorino U, Pasini F, Maissoneuve P, Fraggetta F, Iannucci A, Sonzogni A, De Manzoni G, Terzi A, Durante E, et al. (2003). Independent prognostic value of fascin immunoreactivity in stage I nonsmall cell lung cancer. Br. J. Cancer 88, 537–547. [PubMed: 12592367]

Porporato PE, Payen VL, Perez-Escuredo J, De Saedeleer CJ, Danhier P, Copetti T, Dhup S, Tardy M,Vazeille T, Bouzin C, et al. (2014). A mitochondrial switch promotes tumor metastasis. Cell Rep. 8, 754–766. [PubMed: 25066121]

Reyes A, He J, Mao CC, Bailey LJ, Di Re M, Sembongi H, Kazak L, Dzionek K, Holmes JB, Cluett TJ, et al. (2011). Actin and myosin contribute to mammalian mitochondrial DNA maintenance. Nucleic Acids Res. 39, 5098–5108. [PubMed: 21398640]

Reznik E, Miller ML, Senbabaoglu Y, Riaz N, Sarungbam J, Tickoo SK, Al-Ahmadie HA, Lee W, Seshan VE, Hakimi AA, and Sander C (2016). Mitochondrial DNA copy number variation across human cancers. eLife 5, e10769. [PubMed: 26901439]

Sanjana NE, Shalem O, and Zhang F (2014). Improved vectors and genome-wide libraries for CRISPR screening. Nat. Methods 11, 783–784. [PubMed: 25075903]

Schafer ZT, Grassian AR, Song L, Jiang Z, Gerhart-Hines Z, Irie HY, Gao S, Puigserver P, and Brugge JS (2009). Antioxidant and oncogene rescue of metabolic defects caused by loss of matrix attachment. Nature 461, 109–113. [PubMed: 19693011]

Scott KL, Nogueira C, Heffernan TP, van Doorn R, Dhakal S, Hanna JA, Min C, Jaskelioff M, Xiao Y, Wu CJ, et al. (2011). Proinvasion metastasis drivers in early-stage melanoma are oncogenes. Cancer Cell 20,92–103. [PubMed: 21741599]

Sedeh RS, Fedorov AA, Fedorov EV, Ono S, Matsumura F, Almo SC, and Bathe M (2010). Structure, evolutionary conservation, and conformational dynamics of Homo sapiens fascin-1, an F-actin crosslinking protein. J. Mol. Biol. 400, 589–604. [PubMed: 20434460]

Shukla SK, Purohit V, Mehla K, Gunda V, Chaika NV, Vernucci E, King RJ, Abrego J, Goode GD, Dasgupta A, et al. (2017). MUC1 and HIF-1 alpha signaling crosstalk induces anabolic gluose metabolism to impart gemcitabine resistance to pancreatic cancer. Cancer Cell 32, 71–87.e77. [PubMed: 28697344]

Snyder M, Huang XY, and Zhang JJ (2011). Signal transducers and activators of transcription 3 (STAT3) directly regulates cytokine-induced fascin expression and is required for breast cancer cell migration. J. Biol. Chem. 286, 38886–38893. [PubMed: 21937440]

Sullivan LB, Gui DY, Hosios AM, Bush LN, Freinkman E, and Vander Heiden MG (2015). Supporting Aspartate Biosynthesis Isan Essential Function of Respiration in Proliferating Cells. Cell 162, 552–563. [PubMed: 26232225]

Sun J, He H, Xiong Y, Lu S, Shen J, Cheng A, Chang WC, Hou MF, Lancaster JM, Kim M, and Yang S (2011). Fascin protein is critical for transforming growth factor β protein-induced invasion and filopodia formation in spindle-shaped tumor cells. J. Biol. Chem. 286, 38865–38875. [PubMed: 21914811]

Sun J, He H, Pillai S, Xiong Y, Challa S, Xu L, Chellappan S, and Yang S(2013). GATA3 transcription factor abrogates Smad4 transcription factor-mediated fascin overexpression, invadopodium formation, and breast cancer cell invasion. J. Biol. Chem. 288, 36971–36982. [PubMed: 24235142]

Sun J, Lu F, He H, Shen J, Messina J, Mathew R, Wang D, Sarnaik AA, Chang WC, Kim M, et al. (2014). STIM1- and Orai1-mediated Ca2+ oscillation orchestrates invadopodium formation and melanoma invasion. J. Cell Biol. 207, 535–548. [PubMed: 25404747]

Tilney LG, Connelly PS, Vranich KA, Shaw MK, and Guild GM (1998). Why are two different cross-linkers necessary for actin bundle formation in vivo and what does each cross-link contribute? J. Cell Biol. 143, 121–133. [PubMed: 9763425]

Tsugawa H, Cajka T, Kind T, Ma Y, Higgins B, Ikeda K, Kanazawa M, VanderGheynst J, Fiehn O, and Arita M (2015). MS-DIAL: data-independent MS/MS deconvolution for comprehensive metabolome analysis. Nat. Methods 12, 523–526. [PubMed: 25938372]

Walter P, and Ron D (2011). The unfolded protein response: from stress pathway to homeostatic regulation. Science 334, 1081–1086. [PubMed: 22116877]

Wang W, and Chan JY (2006). Nrf1 istargeted to the endoplasmic reticulum membrane by an N-terminal transmembrane domain. Inhibition of nuclear translocation and transacting function. J. Biol. Chem. 281, 19676–19687. [PubMed: 16687406]

Welsh EA, Eschrich SA, Beglund AE, and Fenstermacher DA (2013). Iterative rank-order normalization of gene expression microarray data. BMC Bioinformatics 14, 153. [PubMed: 23647742]

West AP, Khoury-Hanold W, Staron M, Tal MC, Pineda CM, Lang SM, Bestwick M, Duguay BA, Raimundo N, MacDuff DA, et al. (2015). Mitochondrial DNAstress primesthe antiviral innate immune response. Nature 520, 553–557. [PubMed: 25642965]

Woo DK, Green PD, Santos JH, D'Souza AD, Walther Z, Martin WD, Christian BE, Chandel NS, and Shadel GS (2012). Mitochondrial genome instability and ROS enhance intestinal tumorigenesis in APC(Min/+) mice. Am. J. Pathol. 180, 24–31. [PubMed: 22056359]

Xia J, Mandal R, Sinelnikov IV, Broadhurst D, and Wishart DS (2012). MetaboAnalyst 2.0—a comprehensive server for metabolomics data analysis. Nucleic Acids Res. 40, W127–W133. [PubMed: 22553367]

Yang S, Zhang JJ, and Huang XY (2012). Mouse models for tumor metastasis. Methods Mol. Biol. 928, 221–228. [PubMed: 22956145]

Yang S, Huang FK, Huang J, Chen S, Jakoncic J, Leo-Macias A, Diaz-Avalos R, Chen L, Zhang JJ, and Huang XY (2013). Molecular mechanism of fascin function in filopodial formation. J. Biol. Chem. 288, 274–284. [PubMed: 23184945]

Zhao J, Zhang J, Yu M, Xie Y, Huang Y, Wolff DW, Abel PW, and Tu Y (2013). Mitochondrial dynamics regulates migration and invasion of breast cancer cells. Oncogene 32, 4814–4824. [PubMed: 23128392]

Zhao X, Gao S, Ren H, Sun W, Zhang H, Sun J, Yang S, and Hao J (2014). Hypoxia-inducible factor-1 promotes pancreatic ductal adenocarcinoma invasion and metastasis by activating transcription of the actin-bundling protein fascin. Cancer Res. 74, 2455–2464. [PubMed: 24599125]

Highlights

- Fascin is required for metabolic stress resistance in metastatic lung cancer
- Fascin promotes mitochondrial OXPHOS through remodeling mtF-actin
- Fascin augments the biogenesis of Complex I through mtDNA homeostasis
- The mitochondrial role of fascin is required for it to promote brain metastasis

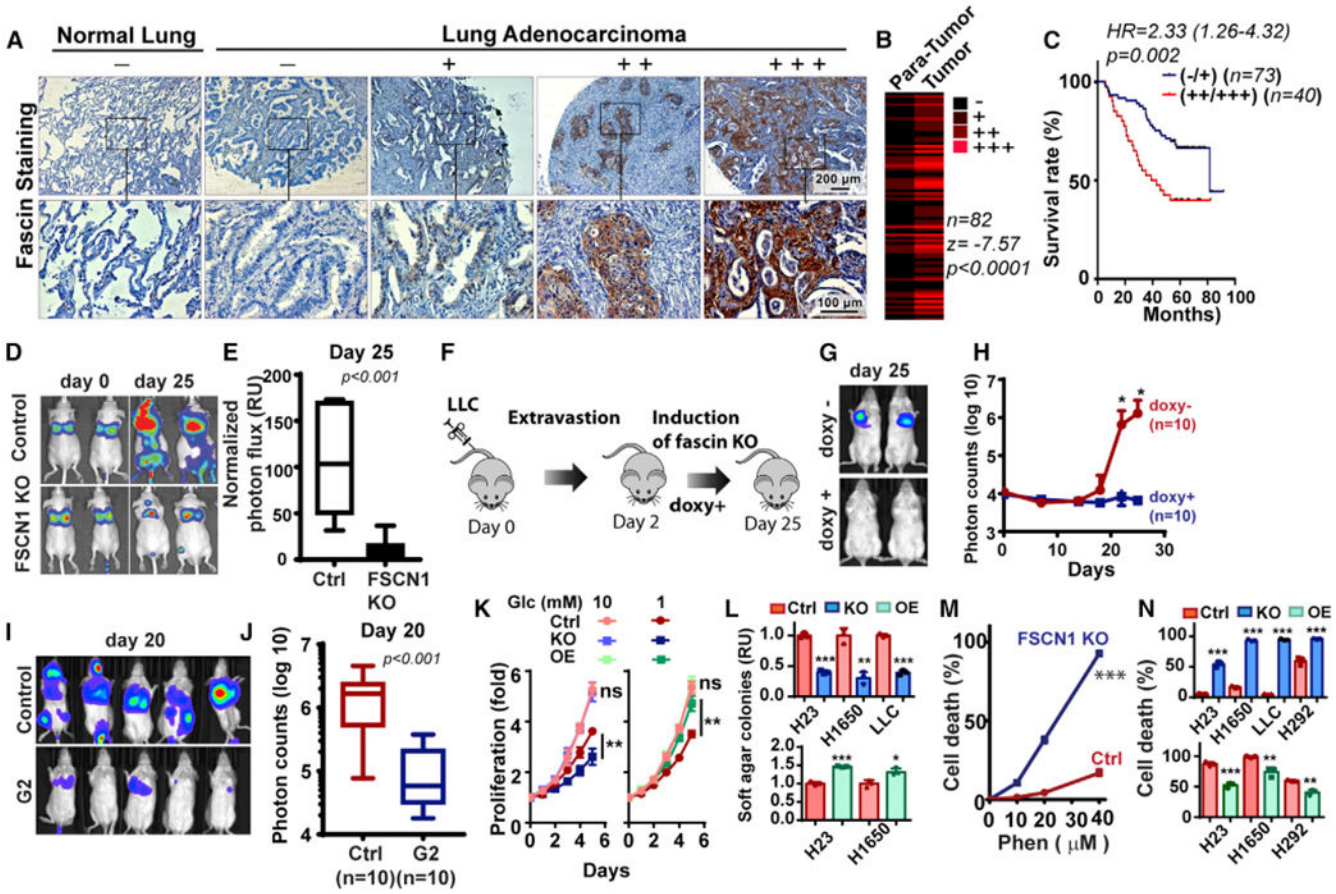

Figure 1. Fascin Is Required for the Metastatic Expansion of NSCLC

(A) Representative IHC staining showing fascin expression in normal lung and lung adenocarcinoma patient specimens.

(B) Expression levels of fascin in 82 pairs of lung adenocarcinoma specimens (tumor) and paired para-tumor lung tissues. p value was determined by two-tailed Wilcoxon signed-rank tests.

(C) The overall survival rate of lung adenocarcinoma patients with low or high fascin expression levels.

(D and E) The effect of fascin knockout on the lung colonization of tail-vein-injected H292 cells (5×10^6). Representative image of bioluminescence imaging (D) and quantitation of photon flux (n = 8, male nude mice) (E) are shown.

(F) Schematics showing inducible fascin KO in extravasated LLC cells with doxycycline chow.

(G and H) Representative bioluminescence imaging (BLI) (day 25) (G) and quantitation (H) (n = 10, female albino BL6 mice), showing that doxycycline (doxy)-induced fascin KO in extravasated LLC cells (2 days post-inoculation) inhibited metastatic expansion.

(I and J) Representative BLI (day 20) (I) and quantitation (J) (n = 10, female albino BL6 mice), showing that fascin inhibitor G2 inhibited metastatic expansion by extravasated LLC cells.

(K) The effects of fascin knockout (KO) or overexpression (OE) on H1650 cell proliferation under different concentrations of glucose in the medium.
(L) Effects of fascin KO or OE on soft agar colony formation in NSCLC cells.
(M) The effects of fascin KO on H1650 cell death when treated with different concentrations of phenformin.
(N) The effects of fascin KO or OE on the sensitivity of NSCLC cell to phenformin-induced cell death.
Data in (C) were analyzed using two-tailed log-rank test; data in (H) and (J)–(N) were analyzed using two-tailed, two-sample unpaired Student's t test. Data in (K)–(N) are representative results from at least three independent experiments (n = 3 biological replicates per group for each experiment).

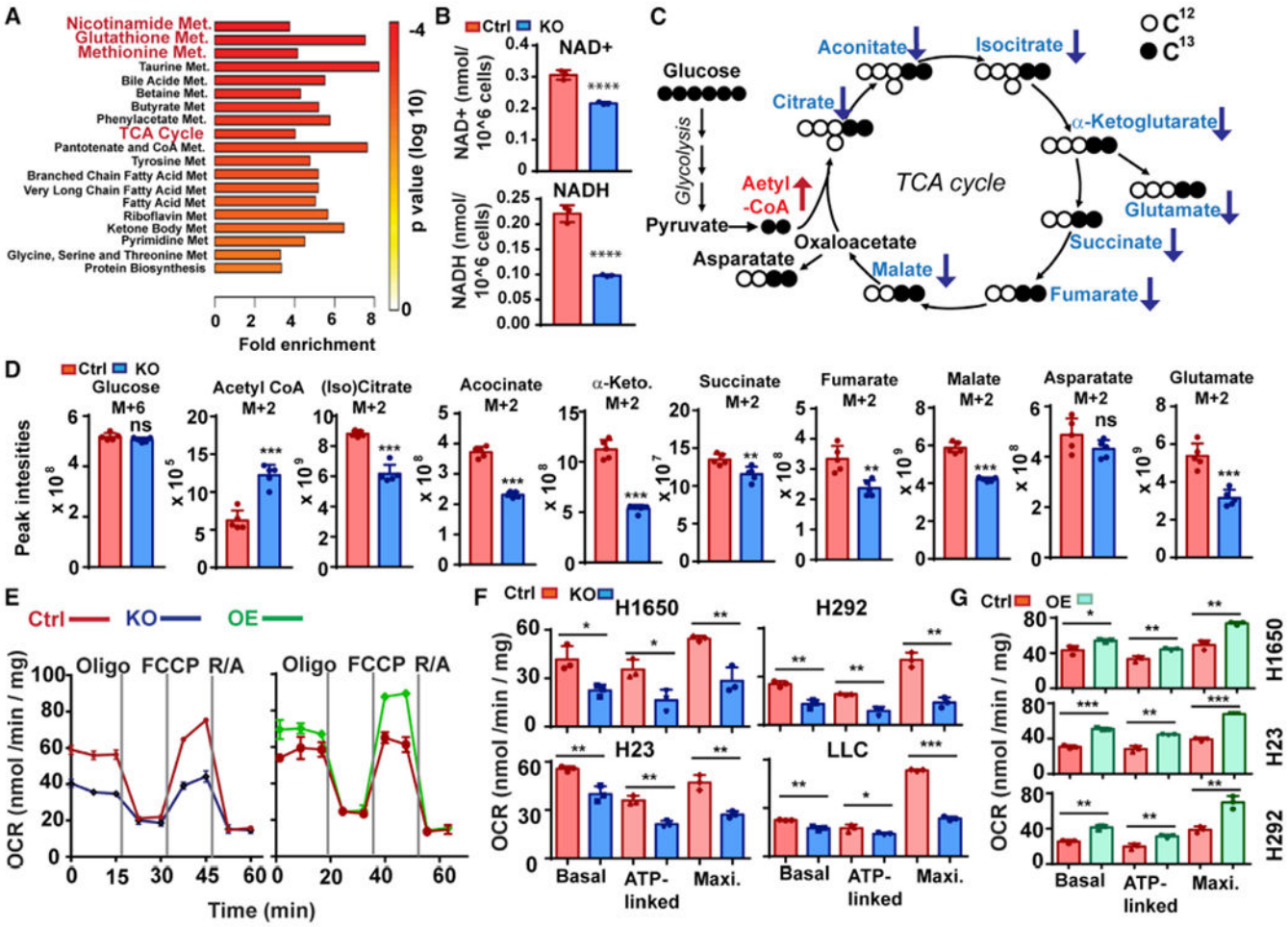

Figure 2. Fascin Is Required for Mitochondrial OXPHOS in NSCLC Cells

(A) The most differentially regulated metabolic pathways in fascin KO H1650 cells.

(B) The effect of fascin depletion on NAD+ and NADH levels in H1650 cells. n = 5 independent samples per group.

(C) Summary of ^{13}C incorporation into TCA cycle metabolites in fascin KO H1650 cells after 6 h of labeling with [U-^{13}C] glucose. Blue and red arrows indicate increases and decreases, respectively, in ^{13}C incorporation into the indicated metabolite.

(D) The levels of ^{13}C incorporation into TCA cycle metabolites in control and fascin KO H1650 cells, as determined by LC-MS analysis. M+x represents the number of ^{13}C-labeled carbon in each metabolite, presented in arbitrary peak intensity units. n = 5 biological replicates per group.

(E) The effects of fascin KO or OE on mitochondrial oxygen consumption rates (OCR), as determined by mito-stress test. n = 3 biological replicates per group.

(F and G) Quantitation of the effects of fascin KO (F) or OE (G) on basal, ATP-linked, and maximum capacity OCR in different NSCLC cell lines.

Data in (B), (D), (F), and (G) were analyzed by two-tailed, two-sample unpaired Student's t test. Representative results from at least three (B and E–G) or two (C and D) independent experiments are shown.

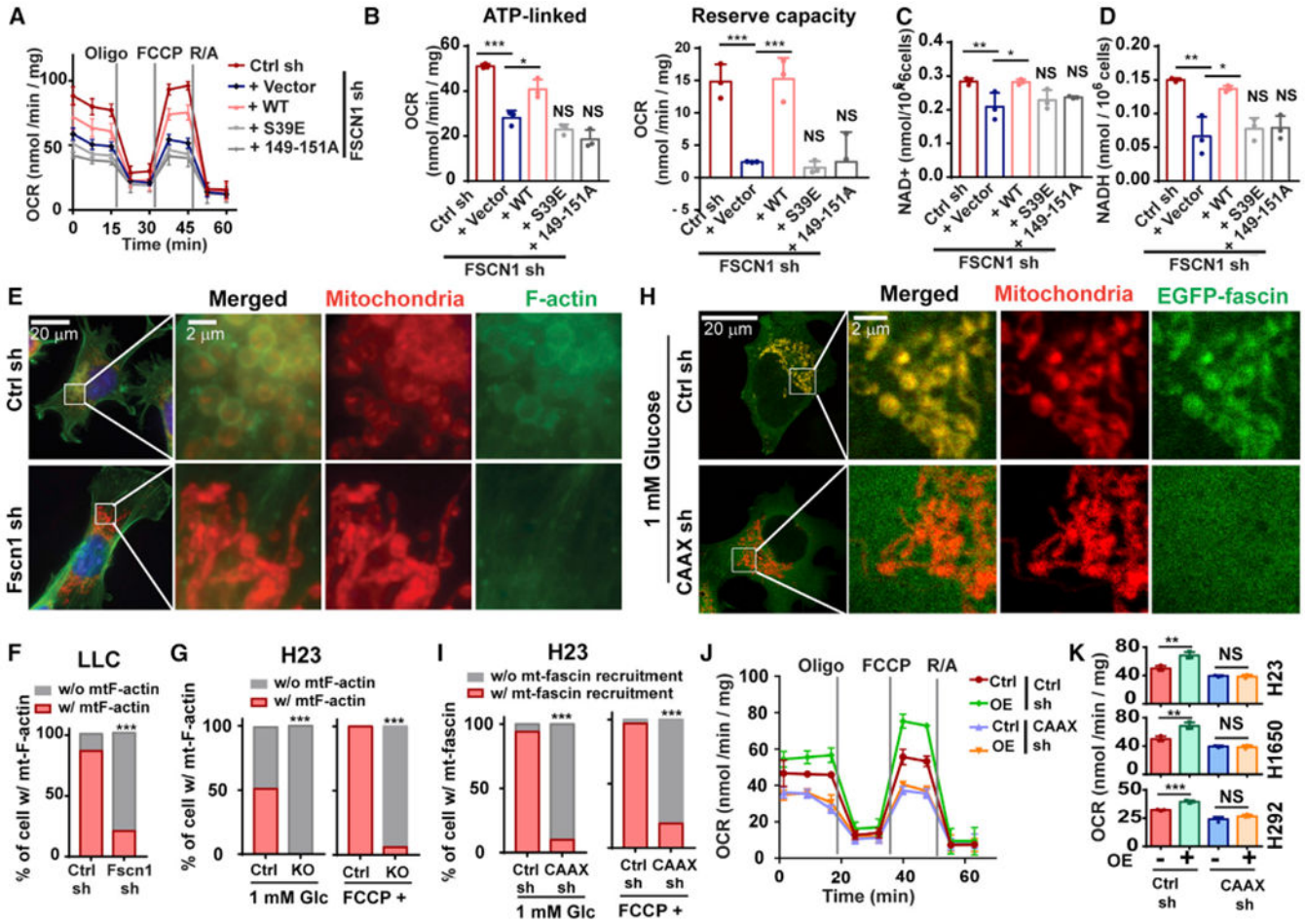

Figure 3. Fascin Controls Mitochondrial OXPHOS by Remodeling mtF-Actin

(A–D) The ectopic expression of wild-type fascin, but not the bundling defective mutants (S39E and 149-151A), in fascin knockdown H1650 cells was able to rescue mitochondrial OCR (A and B) and NAD+ and NADH levels (C and D). n = 3 biological replicates per group.

(E and F) Representative images (E) and quantitation (F) showing constitutive F-actin recruitment to mitochondria in LLC cells.

(G) Quantitation of mitochondrial F-actin in H23 cells under metabolic stress induced by glucose limitation (1 mM glucose [Glc]) or FCCP. n = 30–32 independent l-cell images per group.

(H) Representative images showing the recruitment of EGFP-fascin to mitochondria under glucose limitation and the effects of INF2-CAAX knockdown on fascin recruitment under glucose-limited conditions.

(I) Quantitation of the proportion of control or INF2-CAAX knockdown H23 cells with mitochondrial EGFP-fascin recruitment when subjected to glucose limitation or FCCP treatment. n = 30–32 independent confocal cell images per group.

(J) Mito-stress test showing the effects INF2-CAAX knockdown on fascin-mediated augmentation of mitochondrial OXPHOS in H23 cells. n = 3 biological replicates per group.

(K) Quantitation of the effects of INF2-CAAX knockdown on fascin-mediated augmentation of maximum capacity OCR in three NSCLC cell lines.

Two-tailed, two-sample unpaired Student's t test (for B–D and K or Fisher's exact test (for F, G, and I) were used for analyses. Representative results from at least three independent experiments are shown.

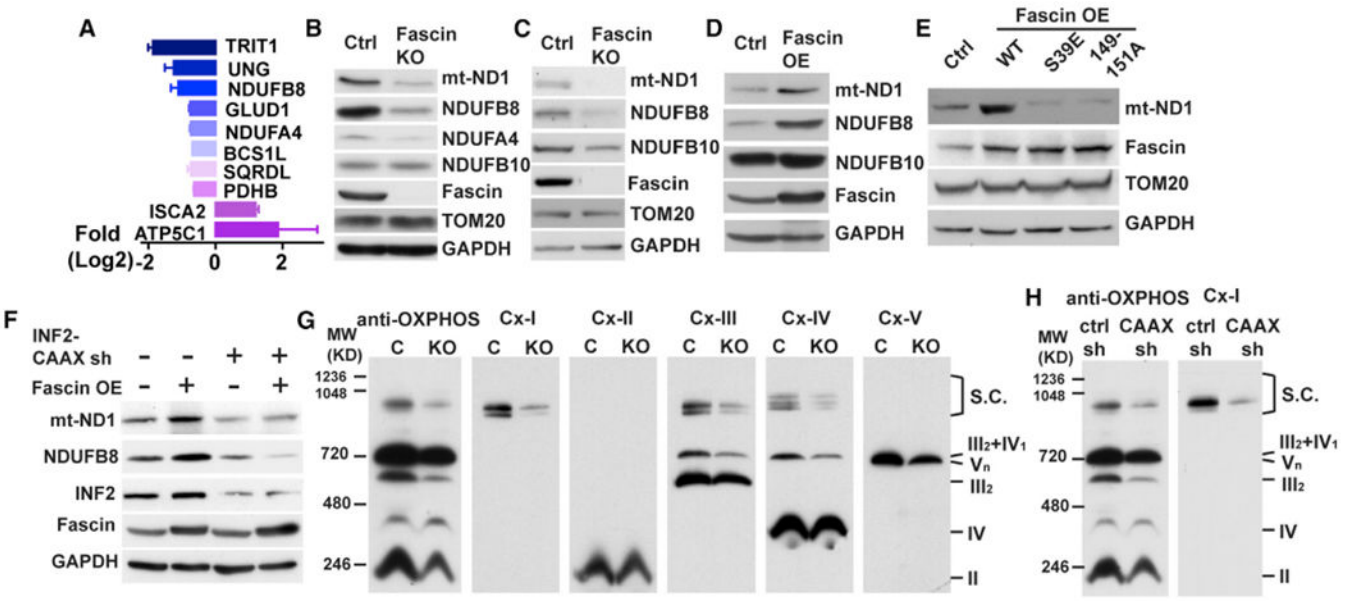

Figure 4. Fascin and mtF-Actin Regulate the Biogenesis of Respiratory Complexes in NSCLC

(A) Waterfall plot showing fold changes of 12 mitochondrial proteins differentially regulated in fascin KO H1650 cells. Fold changes (log_2) are presented as mean ± SEM of results from two independent samples.

(B and C) Western blotting showing the decrease in respiration Complex I subunits in fascin KO H1650 (B) and H23 (C) cells.

(D and E) Western blotting showing the increase in the levels of Complex I subunits in H23 cells overexpressing wild-type fascin (D) but not the S39E and 149-151A mutants (E).

(F) shRNA knockdown of INF2-CAAX abrogated fascin-mediated increase in mt-ND1 and NDUFB8 in H1650 cells.

(G and H) The effect of fascin (G) and INF2-CAAX (H) depletion on the levels of respiratory super complexes in H1650 cells, as determined by BN-PAGE and western blotting using anti-OXPHOS antibody cocktails (recognized all 5 complexes) and antibodies specific for each respiratory complex (Cx I–V). S. C. indicates respirasomes consisting of Complex I, III, and IV.

Representative results from at least three independent experiments are shown.

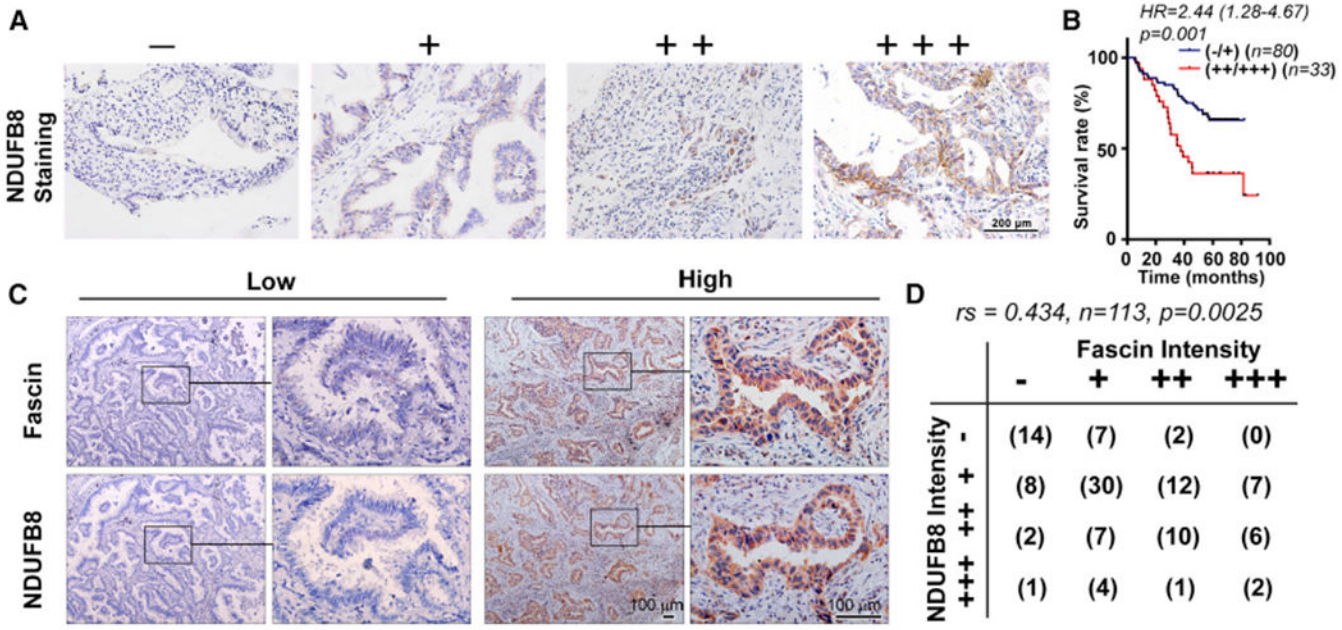

Figure 5. The Correlation between Fascin and NDUFB8 in Lung Cancer Patients

(A) Representative immunohistochemistry staining images showing expression levels of NDUFB8 in lung adenocarcinoma patients.

(B) The survival of lung adenocarcinoma patient with low (−,+) or high (++,+++) NDUFB8 expression. p value and hazard ratio (HR) was determined by two-railed log-rank test.

(C) Fascin and NDUFB8 staining in consecutive sections from lung adenocarcinoma tissue microarray showing the correlation between fascin staining and NDUFB8 staining.

(D) Correlation between fascin and NDUFB8 staining intensities in lung adenocarcinoma tissue microarray.

Correlation coefficient and p value were calculated by Spearman correlation test.

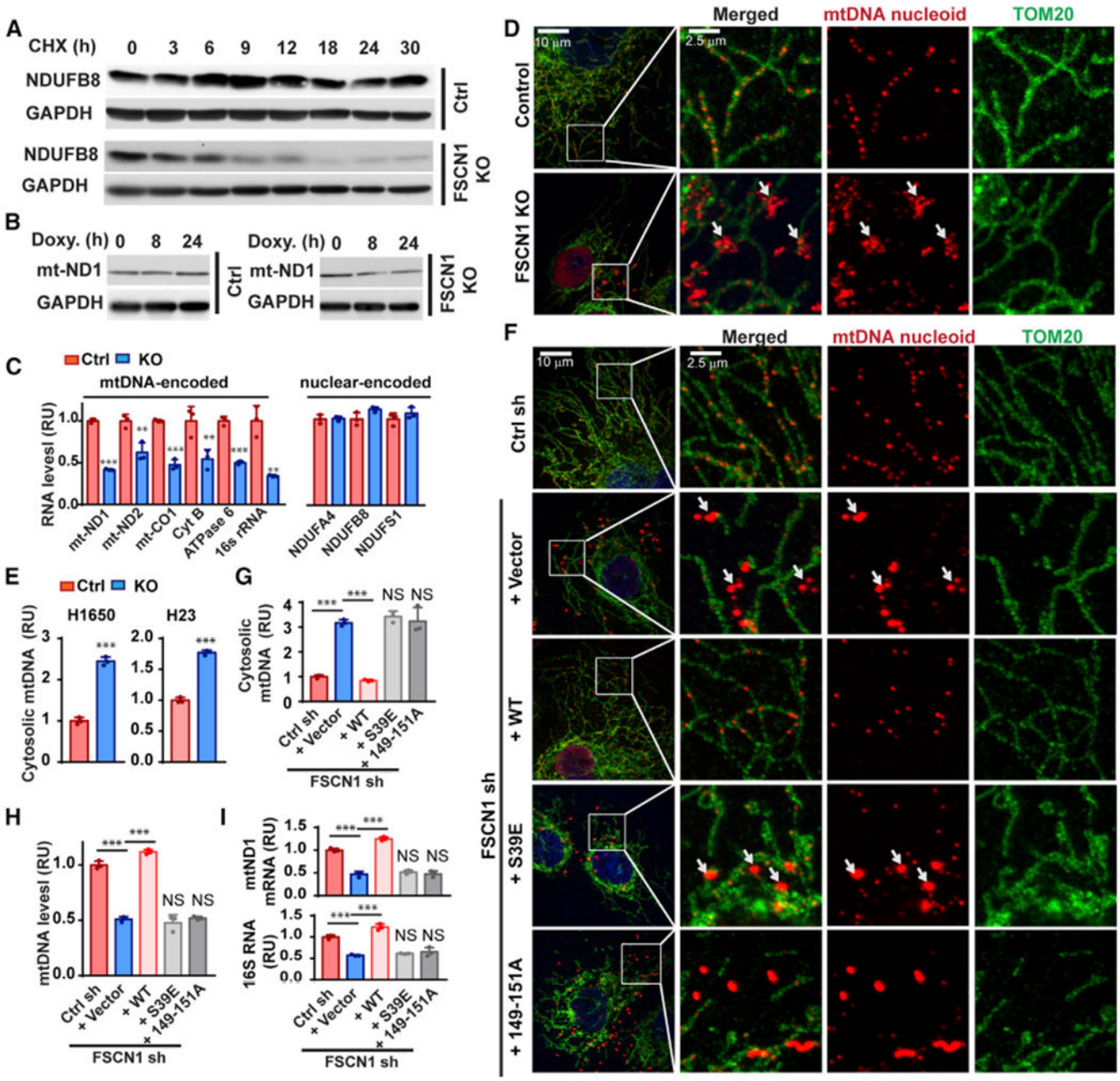

Figure 6. Fascin and mtF-Actin Are Required for mtDNA Maintenance in NSCLC

(A and B) H23 cells were treated with the eukaryotic ribosome inhibitor cycloheximide (CHX) (A) or mitochondrial ribosome inhibitor doxycline for the indicated time (B), and the protein levels of NDUFB8 and mt-ND1were determined by western blotting.

(C) Fascin KO decreased the mRNA levels of mtDNA-encoded respiration complex subunits (Complex I: mt-ND1, mt-ND2; Complex III: mt-CO1; Complex IV: CytB; and Complex V: ATPase 6), mitochondrial ribosome 16S rRNA, without affecting the levels of nuclear-encoded NDUFA4, NDUFB8, and NDUFS1 in H23 cells. n = 3 biological replicates per group.

(D) Representative images showing mtDNA nucleoid (anti-DNA, red) and mitochondrial staining (Tom20, green) in control and fascin KO H1650 cells. Arrows indicate mtDNA nucleoid aggregates.
(E) The levels of cytosolic mtDNA in control and fascin KO NSCLC cells, as determined by qPCR. n = 3 biological replicates per group.
(F) Representative images showing the effects of ectopically expressed wild-type fascin or bundling-defective mutants (S39E and 149-151A) on mtDNA aggregation in fascin-depleted H1650 cells. Arrows indicate mtDNA nucleoid aggregates.
(G) Quantitation of the percentage of cells with mtDNA nucleoid aggregate in (F).
(H and I) qPCR quantitation of the levels of mtDNA (H) or mtDNA-encoded RNA transcripts (I) in control, fascin knockdown, or knockdown-rescue H1650 cells.
Data in (C), (E), and (G)–(I) were analyzed by two-tailed, two-sample unpaired Student's t test. NS, statistically not significant. Representative results from at least three independent experiments are shown.

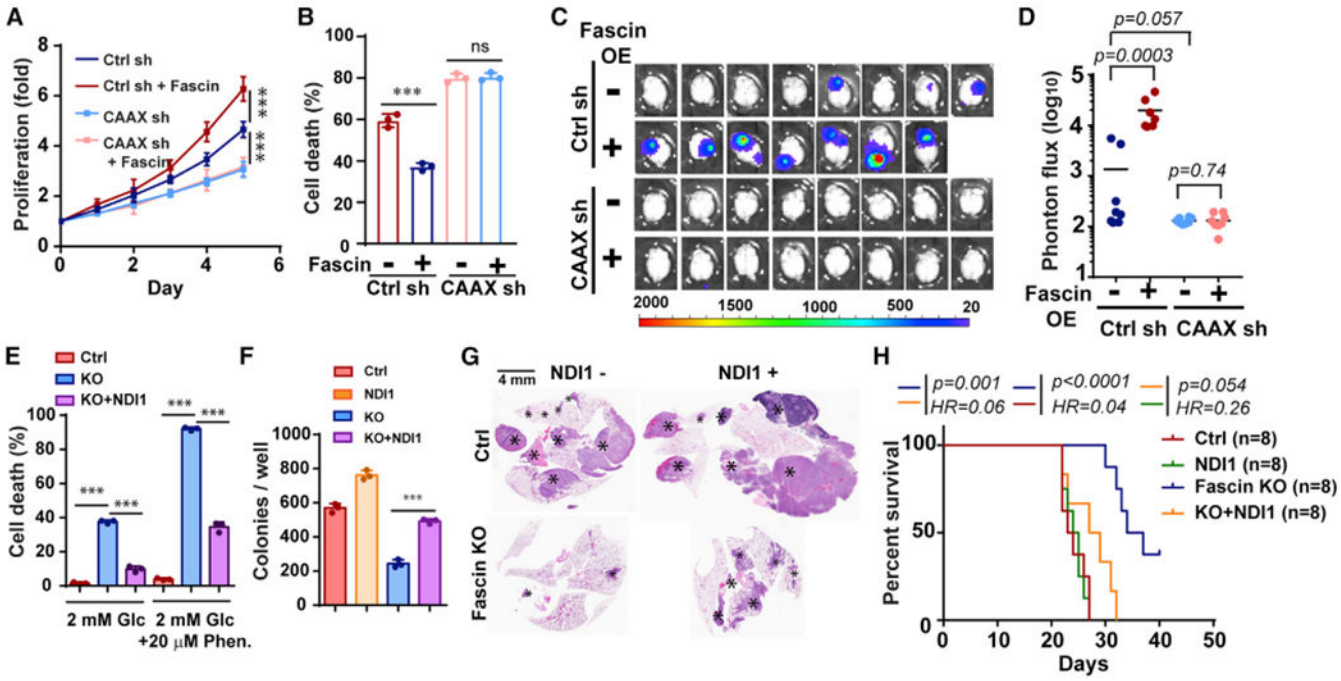

Figure 7. Fascin Promotes Metabolic Stress Resistance and Lung Cancer Metastasis by Remodeling mtF-Actin and Augmenting Mitochondrial OXPHOS

(A and B) The effects of fascin OE and INF2-CAAX knockdown on the resistance of H1650 cells to glucose limitation (1mM glucose) (A) and phenformin (B). n = 3 independent samples per group.

(C and D) *Ex vivo* bioluminescence imaging (C) and quantitation of photon flux (D) showing the effects of fascin OE and INF2-CAAX knockdown on H292 brain metastasis in nude mice. n = 7 or 8 mice, as indicated, per group.

(E and F) The effects of fascin KO and ectopic NDI1 expression on cell proliferation under glucose-limited conditions (1mM glucose) (E) and soft-agar colony formation (F) in LLC cells. n = 3 biological replicates per group.

(G and H) Representative H&E staining (G) and survival analysis (H) showing the effects of fascin KO and ectopic NDI1 expression on lung metastasis by tail-veininjected LLC cells. n = 8, two-tailed log-rank test.

Representative results from at least three independent experiments are shown in (A), (B), (E), and (F). Data were analyzed by two-tailed, two-sample unpaired Student's t test.

KEY RESOURCES TABLE

REAGENT or RESOURCE	SOURCE	IDENTIFIER
Antibodies		
Fascin 1 Antibody (55K-2)	Santa Cruz	Cat# SC-21743, RRID:AB_627580
Tom20 Antibody (FL-145)	Santa Cruz	SC-11415, RRID:AB_2207533
DRP1 Antibody (C-5)	Santa Cruz	SC-271583, RRID:AB_10659110
Anti-Rabbit, HRP	Cell Signaling	7074s, RRID:AB_2099233
Anti-Mouse, HRP	Cell Signaling	7076s, RRID:AB_330924
INF2 antibody	Millipore	ABT61, RRID:AB_11203139
Monoclonal Anti-GAPDH antibody	Sigma	G8795, RRID:AB_1078991
NDUFB8 antibody (20E9DH10C12)	Thermo Scientific	459210, RRID:AB_2532232
NDUFA4 antibody	Thermo Scientific	PA5-51021, RRID:AB_2636469
MT-ND1 antibody	Novus	NBP100939, RRID:AB_1503736
NDUFB10 antibody	Thermo Scientific	PA5-51179, RRID:AB_2636627
OXPHOS Complex Monoclonal antibody (Cocktail)	Thermo Scientific	45-7999, RRID:AB_2533834
Complex I NDUFA9 20C11B11B11	Thermo Scientific	459100, RRID:AB_2532223
Complex II SDHA antibody (2E3GC12FB2AE2)	Thermo Scientific	459200, RRID:AB_2532231
Complex III UQCRC2 antibody [13G12AF12BB11]	Abcam	ab14745, RRID:AB_2213640
Complex IV MTCO1 antibody [1D6E1A8]	Abcam	ab14705, RRID:AB_2084810
Complex V ATP5A1 antibody (15H4C4)	Thermo Scientific	43-9800, RRID:AB_2533548
Anti-DNA antibody, clone AC-30-10	Millipore	CBL186, RRID:AB_93367
Anti-cytochrome *c* antibody	Cell Signaling	4272, RRID:AB_2090454
Alexa 488 goat anti-mouse	Thermo Scientific	A11001, RRID:AB_2534069
Alexa 594 goat anti-mouse	Thermo Scientific	A11032, RRID:AB_141672
Alexa 488 goat anti-rabbit	Thermo Scientific	A11008, RRID:AB_143165
Alexa 594 goat anti-rabbit	Thermo Scientific	A11012, RRID:AB_2534079
Alexa Fluor® 555 Mouse anti-Cytochrome *c* Clone 6H2.B4 (RUO) BD	BD Biosciences	558700, RRID:AB_1645293
ANTI-FLAG® M2 antibody	Sigma	F3165, RRID:AB_259529
PLS3 (Fimbrin) antibody	Thermo Scientific	PA5-27883, RRID:AB_2545359)
Cortactin antibody	Millipore	05-180, RRID:AB_309647
Bacterial and Virus Strains		
Stable Competent *E. coli* (High Efficiency)	NEB	C3040I
pLenti-CMV-blasticidin	Campeau et al., 2009	Addgene_17486
pLV-mitoDsRed	Kitay et al., 2013	Addgene_44386
pLX304-PLS3 (Fimbrin)	Harvard Plasmids	NP_001129497.1
pLenti-PGK V5-LUC Neo (w623-2)	Campeau et al., 2009	Addgene_21471
pLenti-CRISPR V2 vector	Sanjana et al., 2014	Addgene_52961
pLKO-DNM1L (DRP1) shRNA1	Sigma	TRCN0000318424
pLKO-DNM1L (DRP1) shRNA2	Sigma	TRCN0000318425

REAGENT or RESOURCE	SOURCE	IDENTIFIER
pLenti-Guide-Puro	Sanjana et al., 2014	Addgene_52963
pLenti CMV rtTA3 Blast (w756-1)	Eric Campeau	Addgene_26429
pLenti CMVtight Hygro DEST (w769-1)	Eric Campeau	Addgene_26433
pLNCX2-mApple-Lifeact	Sun et al., 2014	Addgene_89820
pX330-U6-Chimeric_BB-CBh-hSpCas9	Cong et al., 2013	Addgene_42230
Biological Samples		
A total of 113 sequential lung adenocarcinoma tumor tissues were collected from patients	Tianjin Medical University Cancer Institute and Hospital	N/A
Another set of 82 pairs of lung adenocarcinoma tumor tissues and corresponding adjacent non-tumor tissues were collected from patients	Tianjin Medical University Cancer Institute and Hospital	N/A
Chemicals, Peptides, and Recombinant Proteins		
Fetal Bovine Serum	Atlanta Biological	S11150
Penicillin/Streptomycin	GIBCO	15140163
DMEM Medium	HyClone	SH30243.FS
DMEM Medium, no glucose	GIBCO	11966025
RPMI 1640 Medium	HyClone	SH30027.FS
RPMI 1640 Medium, no glucose	GIBCO	11879020
FCCP	Abcam	NC0474145
Blebbistatin	Sigma	B0560
Doxycycline	Fisher Scientific	BP2653-1
Cycloheximide (CHX)	Sigma	C7698
Protease inhibitors cocktail	Roche	04693159001
Phosphatase inhibitor cocktail	Thermo Scientific	88667
Fluoromount	Sigma	F4680
DAPI (4’,6-Diamidino-2-Phenylindole, Dihydrochloride)	Thermo Scientific	D1306
NativePAGETM precast gel	Thermo Scientific	BN1001BOX
NativePAGETM running buffer	Thermo Scientific	BN2001
NuPAGETM transfer buffer	Thermo Scientific	NP00061
Brilliant Blue G	Sigma	B0770
PVDF Transfer Membranes	Millipore	IPVH00010
Methanol	Fisher Scientific	BP11054
Low melting agar	Fisher Scientific	BP165-25
iodonitrotetrazolium chloride	Biosynth,	I-7630
Formalin 10%	Fisher Scientific	SF100-4
Paraformaldehyde	Sigma	158127
Crystal violet solution	Eng Scientific	INC NO. 6100
Propidium iodide	Sigma	P4170
Digitonin	EMD	
DyLight 488 Lycopersicon Esculentum Lectin	Vector Laboratories	DL-1174
D-Luciferin Sodium Salt	Regis Tech	103404-75-7

REAGENT or RESOURCE	SOURCE	IDENTIFIER
Doxycycline chow	BioServ	S3888
G2 inhibitor	Enamine	EN300-246105
D-Glucose-^{13}C6	Sigma	389374
CK-666	Sigma	SML0006
Phenformin hydrochloride	Sigma	P7045
DNase I, RNase-free	Thermo Scientific	EN0525
Critical Commercial Assays		
NAD+ /NADH Assay Kit	Biovision	k337-100
DAB Peroxidase (HRP) Substrate Kit	Vector	SK-4100
NativePAGE Sample Prep Kit	Thermo Scientific	BN2008
XF Cell Mito Stress Test Kit	Agilent	103015-100
RNeasy Kit	QIAGEN	74106
DNeasy Kit	QIAGEN	69504
ABI qPCR master mix	Thermo Scientific	4367659
Experimental Models: Cell Lines		
H1650	ATCC	CRL-5883
H23 (microbial (including mycoplasma) verified free)	Moffitt Cancer Center	N/A
H292	ATCC	CRL-1848
LLC (microbial (including mycoplasma) verified free)	Moffitt Cancer Center	N/A
HEK293	ATCC	CRL-1573
Experimental Models: Organisms/Strains		
B6 Albino Mouse	Charles River	Strain Code 493
NU/NU Nude Mouse	Charles River	Strain Code 088
Oligonucleotides		
See Table S4		
Recombinant DNA		
pLNCX2-EGFP-Fascin1 human	This paper	N/A
pSUPER.Retro.puro-Fascin1 (human/mouse): GGTGGGCAAAGATGAGCTC	Sun et al., 2011	N/A
pSUPER.Retro.puro-shINF2-CAAX: ACAAAGAAACTGTGTGTGA	This paper	N/A
pSUPER.Retro.puro-Cortactin sh1: GGTTTCGGCGGCAAATACG	This paper	N/A
pSUPER.Retro.puro-Cortactin sh2: CGAATATCAGTCGAAACTT	This paper	N/A
pLenti-CRISPR V2-puro-Fascin1 human: GAAGAAGCAGATCTGGACGC	This paper	N/A
pLenti-CRISPR V2-puro-Fascin1 mouse: TCGCTACCTGGCCGCCGACA	This paper	N/A
pLenti-CMV-Fascin1 wt human	This paper	N/A
pLenti-CMV-Fascin1 s39e human	This paper	N/A
pLenti-CMV-Fascin1 149-151A human	This paper	N/A

REAGENT or RESOURCE	SOURCE	IDENTIFIER
pLenti CMVtight -Cas9 Hygro	This paper	N/A
Software and Algorithms		
MS-DIAL	Tsugawa et al., 2015	http://prime.psc.riken.jp/Metabolomics_Software/MS-DIAL/
MaxQuant	Cox and Mann, 2008	https://maxquant.org
Metaboanalyst 2.0	Xia et al., 2012	https://www.metaboanalyst.ca
Prism	GraphPad	Version 7